Atmos. Chem. Phys., 13, 463–486, 2013
www.atmos-chem-phys.net/13/463/2013/
doi:10.5194/acp-13-463-2013

Atmospheric Chemistry and Physics

Using measurements of the aerosol charging state in determination of the particle growth rate and the proportion of ion-induced nucleation

J. Leppä[1], S. Gagné[2,*], L. Laakso[1,2,3], H. E. Manninen[2], K. E. J. Lehtinen[4], M. Kulmala[2], and V.-M. Kerminen[2]

[1]Finnish Meteorological Institute, P.O. Box 503, 00101 Helsinki, Finland
[2]Department of Physics, P.O. Box 64, 00014, University of Helsinki, Finland
[3]School of Physical and Chemical Sciences, North-West University, Private Bag x6001, Potchefstroom 2520, South Africa
[4]Finnish Meteorological Institute, Kuopio Unit, and University of Eastern Finland, Department of Applied Physics, P.O. Box 1627, 70211 Kuopio, Finland
[*]now at: Department of Physics and Atmospheric Science, Dalhousie University, Halifax, B3H 3J5, Canada and at Environment Canada, Downsview, Toronto, M3H 5T4, Canada

Correspondence to: J. Leppä (johannes.leppa@fmi.fi)

Received: 11 July 2012 – Published in Atmos. Chem. Phys. Discuss.: 24 August 2012
Revised: 5 December 2012 – Accepted: 18 December 2012 – Published: 15 January 2013

Abstract. The fraction of charged nucleation mode particles as a function of particle diameter depends on the particle growth rate and the proportion of particles formed via ion-induced nucleation. In this study we have tested the applicability of recent data analysis methods to determine the growth rate and the proportion of ion-induced nucleation from the measured charged fractions. For this purpose we have conducted a series of aerosol dynamic simulations covering a wide range of atmospheric conditions. The growth rate and initial fraction of charged particles were estimated from simulated data using these methods and compared with the values obtained directly from the simulations. We found that the data analysis methods used in this study should not be used when the nuclei growth rate is less than $\sim 3\,\mathrm{nm\,h^{-1}}$, or when charged particles grow much more rapidly than neutral ones. Furthermore, we found that the difference in removal rates of neutral and charged particles should be taken into account when estimating the proportion of ion-induced nucleation. Neglecting the higher removal rate of charged particles compared with that of neutral ones could result in an underestimation of the proportion of ion-induced nucleation by up to a factor of 2. This underestimation is further increased if charged particles grow more rapidly than neutral ones. We also provided a simple way of assessing whether these methods are suitable for analyzing data measured under specific conditions. The assessment procedure was illustrated using a few examples of actual measurement sites with a more detailed examination of the typical conditions observed at the SMEAR II station in Hyytiälä, Finland.

1 Introduction

Aerosol particles affect the radiative forcing budget of the atmosphere directly by scattering solar radiation and indirectly by affecting the properties of clouds (Seinfeld and Pandis, 2006). Recent studies suggest that atmospheric nucleation is the dominant source of the aerosol particles in the atmosphere (Spracklen et al., 2006; Kulmala and Kerminen, 2008; Yu et al., 2010). The number of particles of climatically-relevant sizes formed via nucleation depends on three factors: the nucleation rate, the nuclei growth rate and the scavenging of nuclei by various removal processes (Kerminen et al., 2001; Lehtinen et al., 2007; Pierce and Adams, 2007; Kuang et al., 2009; Gong et al., 2010). The growth rate of sub-20 nm nuclei is of specific interest in this regard, since these particles are most susceptible for coagulation scavenging by larger pre-existing particles.

The exact mechanisms of atmospheric nucleation are not yet completely known (e.g. Kerminen et al., 2010; Kulmala et al., 2011), but the proposed mechanisms can be divided into two categories: the neutral ones and the ones involving one or more electric charges. The latter include, but are not restricted to, ion-induced nucleation (IIN), in which a particle is formed by the activation of a charged small ion (a large molecule or a molecular cluster). By activation, we mean a process by which the ion reaches a size at which it is more likely to grow to larger sizes by condensation of vapours onto the particle surface than decrease in size through evaporation. In laboratory conditions, the ions have been observed to be activated at lower vapour concentrations than similarly-sized neutral molecules or clusters and, furthermore, a sign preference in activation of the ions has been observed (Winkler et al., 2008). As a result, some particles in the atmosphere may be formed via IIN while others are formed via neutral mechanisms. According to field measurements, the fraction of IIN to the total nucleation rate varies from one place to another (Manninen et al., 2010), as well as from one day to another (Laakso et al., 2007a; Gagné et al., 2008, 2010), and even during a continuous nucleation event (Laakso et al., 2007b). The contribution of IIN to new particle formation is important from a climate change point of view, since most of the uncertainty in global-average radiative forcing is caused by aerosol effects (Forster et al., 2007).

After their formation, neutral particles can be charged by ion-aerosol attachment or by coagulation with charged particles. Similarly, charged particles can be neutralized by recombination with oppositely-charged particles or small ions ($< \sim 1.8$ nm in diameter). As a result, the fraction of particles carrying a charge changes, until charging and neutralization of the particles are at a balance, which will be denoted as the charge equilibrium in this study.

According to observations, concentrations of negatively- and positively-charged small ions are usually of the same order of magnitude and often even quite close to each other, but there are also quite many observations of substantially different concentrations of negatively- and positively-charged small ions (Hirsikko et al., 2011). In this study, the term "asymmetric small ion concentrations" is used to denote that the concentrations of negatively- and positively-charged small ions are different.

Kerminen et al. (2007) derived equations describing the diameter dependence of the aerosol charging state, which has been used to estimate the amount of IIN from measurement data (e.g. Laakso et al., 2007a; Gagné et al., 2008). Iida et al. (2008) derived similar equations for the charged fraction, which were then used to determine the particle diameter growth rate (GR). In the studies by Kerminen et al. (2007) and Iida et al. (2008), the concentrations of negatively- and positively-charged small ions ($< \sim 1.8$ nm) were assumed to be the same. Furthermore, the fractions of negatively- and positively-charged particles ($> \sim 1.8$ nm) were assumed to be the same and the recombination and attachment coefficients were assumed to be the same for negatively- and positively-charged small ions. As a result, the negative and positive equilibrium charged fractions and charging states were the same.

In the study by Gagné et al. (2012), the methods for estimating the proportion of IIN and GR were modified for conditions in which the negative and positive small ion concentrations and charged fractions are not the same, termed the "asymmetric framework". Also the attachment coefficients were allowed to differ for negative and positive small ions.

Numerous simplifying assumptions have been made when developing the methods discussed above (Kerminen et al., 2007; Iida et al., 2008; Gagné et al., 2012), and the justification of these assumptions under certain conditions has been presented in the corresponding studies. However, it is extremely difficult to estimate the precision of the results obtained with these methods by using them on the measured data, since the growth rate and fractions of IIN are either not known or they have to be estimated with some other methods that include uncertainties of their own. In this work, we have used these analysis methods for data obtained from aerosol dynamic simulations with a known particle growth rate and fractions of IIN.

The main goal of this paper is to explore the conditions in which the particle diameter growth rate and the proportion of IIN can be reliably determined from the charged fractions using the methods described by Gagné et al. (2012). Specifically, we aim to address the effect of the following conditions on the precision of the methods used in this study: (1) charged particles growing more rapidly than neutral ones, (2) particles growing by a diameter dependent rate, (3) coagulation processes having a significant effect in the evolution of particle size distribution and (4) negative and positive small ions having different concentrations (asymmetry).

To begin with, we will shortly describe the data analysis methods used to estimate the particle growth rate and the fraction of particles formed carrying a charge and the theory they are based on. These methods will then be used on data obtained from a set of aerosol dynamics simulations. The precision of the methods will be assessed by comparing the estimated values with the corresponding values obtained directly from simulations.

2 Theoretical background

2.1 Definitions used in this study

In this study, we will use the asymmetric framework described by Gagné et al. (2012), in which the concentrations of negatively- and positively-charged small ions as well as negatively- and positively-charged particles are allowed to be different. Furthermore, the attachment coefficients of negatively- and positively-charged small ions to neutral particles, as well as the recombination coefficients of small ions

with oppositely-charged particles, are allowed to have different values.

Let us consider a system that consists of two aerosol particle modes: a narrow nucleation mode and a mode of larger pre-existing particles. The fraction of negatively- (positively-) charged particles, f^- (f^+), is defined as the ratio of the concentration of negatively- (positively-) charged nucleation mode particles to the total (charged + neutral) nucleation mode particle concentration, $f^\pm = N^\pm/N^{\mathrm{tot}}$. If the particle number concentrations of both of the modes are sufficiently small, the coagulation processes are negligible and the fraction of charged particles changes mainly due to ion-aerosol attachment. Furthermore, in a case of a non-growing nucleation mode, the fraction of charged particles approaches a steady state value, which is denoted as the equilibrium charged fraction, $f_{\mathrm{eq}}^\pm$, in this study. With these assumptions, the equilibrium charged fraction can be estimated by (Gagné et al., 2012):

$$f_{\mathrm{eq}}^\pm\left(d_\mathrm{p}\right) \approx \frac{\beta^\pm\left(d_\mathrm{p}\right)\times N_\mathrm{C}^\pm}{\alpha^\mp\left(d_\mathrm{p}\right)\times N_\mathrm{C}^\mp+\beta^\pm\left(d_\mathrm{p}\right)\times N_\mathrm{C}^\pm+\beta^\mp\left(d_\mathrm{p}\right)\frac{\left(N_\mathrm{C}^\mp\right)^2}{N_\mathrm{C}^\pm}} \approx \frac{\beta^\pm\left(d_\mathrm{p}\right)\times N_\mathrm{C}^\pm}{\alpha^\mp\left(d_\mathrm{p}\right)\times N_\mathrm{C}^\mp}. \quad (1)$$

Here N_C^- and N_C^+ are the concentrations of negatively- and positively-charged small ions, respectively, α^q is the recombination coefficient of a small ion carrying a charge q with an oppositely-charged particle, β^q is the attachment coefficient of a small ion carrying a charge q to a neutral particle, and d_p is the particle diameter.

The aerosol charging state, $S^\pm$, is in turn defined as the ratio of the fraction of charged particles to the fraction of charged particles in the charge equilibrium (Kerminen et al., 2007):

$$S^\pm\left(d_\mathrm{p}\right) = \frac{f^\pm\left(d_\mathrm{p}\right)}{f_{\mathrm{eq}}^\pm\left(d_\mathrm{p}\right)}. \quad (2)$$

2.2 Methods to determine the growth rate and initial charged fraction

Here we will describe two methods that can be used to determine the particle diameter growth rate and the charged fraction at the size of particle formation. Both of these methods are based on the behaviour of the fraction of charged particles as a function of diameter.

2.2.1 The fitting method

The aerosol charging state, $S^\pm(d_\mathrm{p})$, has the following dependence on the particle diameter (Kerminen et al., 2007; Gagné et al., 2012):

$$S^\pm\left(d_\mathrm{p}\right) = 1-\frac{1}{K^\pm d_\mathrm{p}}+\frac{\left(S_0^\pm-1\right)K^\pm d_0+1}{K^\pm d_\mathrm{p}}e^{-K^\pm\left(d_\mathrm{p}-d_0\right)}, \quad (3)$$

where

$$K^\pm = \frac{\alpha N_\mathrm{C}^\mp}{\mathrm{GR}}. \quad (4)$$

Here d_p is the particle diameter, $S_0^\pm$ is the negative or positive charging state at diameter d_0 and GR is the particle diameter growth rate. The recombination coefficient, α, is assumed to be constant with the value of $1.6\times10^{-6}\,\mathrm{cm^3\,s^{-1}}$ (Nolan, 1941) used in this study. Here it should be noted that the parameter $K^\pm$ related to the negative or positive charging state depends on the concentration of oppositely-charged small ions ($K^\pm \propto N_\mathrm{C}^\mp$).

Let us assume that we have data points (measured or simulated) of the charging state for a certain range of particle diameter. Now, we can estimate the charging state, $S_0^\pm$, at any size d_0 by fitting Eq. (3) to the data points using $S_0^\pm$ and $K^\pm$ as the fitting parameters. The fitting can be done separately for negative and positive polarities. By setting d_0 to be the size at which we assume that particle formation occurs, the fitting provides us an estimate on the initial charging state of the freshly-formed particle population. Furthermore, using Eqs. (1) and (2), we can estimate the initial charged fraction, $f_{\mathrm{ini}}^\pm$ ($f_{\mathrm{ini}}^\pm = f^\pm(d_0)$), from the initial charging state and using Eq. (4), we can estimate the particle growth rate from the parameter $K^\pm$. Here GR is assumed to be constant with the particle diameter and the same for neutral and charged particles. In this paper, this procedure is called the fitting method.

2.2.2 The iteration method

The following equations describe the behaviour of positive and negative charged fractions as a function of diameter (Gagné et al., 2012):

$$\left(\frac{\mathrm{d}f^-}{\mathrm{d}d_\mathrm{p}}\right) = \mathrm{GR}^{-1}\left(\left(1-f^--f^+\right)\beta^-N_\mathrm{C}^- - \alpha^+f^-N_\mathrm{C}^+\right) \quad (5)$$

$$\left(\frac{\mathrm{d}f^+}{\mathrm{d}d_\mathrm{p}}\right) = \mathrm{GR}^{-1}\left(\left(1-f^--f^+\right)\beta^+N_\mathrm{C}^+ - \alpha^-f^+N_\mathrm{C}^-\right). \quad (6)$$

Here it should be noted that, contrary to the fitting method described above, the recombination coefficient, $\alpha^\pm$, between a small ion and an oppositely-charged particle is assumed to depend on the particle diameter and also to be different for negative and positive small ions.

By choosing the value of GR and the values of the charged fractions, f_0^- and f_0^+, at the chosen diameter d_0, we can calculate the charged fractions as a function of diameter by simultaneously solving Eqs. (5) and (6). Now, let us assume that we have data points (measured or simulated) of the charged fraction in a certain range of particle diameter. By iteratively changing the values of GR, f_0^- and f_0^+ when solving Eqs. (5) and (6), we can search for the best correspondence between the calculated values of charging state and the data points. By setting d_0 to be the size at which we assume

that the particle formation occurs, we get an estimate on GR and the initial charged fraction of the freshly-formed particle population, $f_{\mathrm{ini}}^{\pm}$. Here GR is assumed to be constant with the particle diameter and the same for neutral and charged particles. In this study, this procedure is called the iteration method.

If we are only interested in GR, but not in $f_{\mathrm{ini}}^{\pm}$, we can set d_0 to be the smallest diameter for which we have the data on the charged fractions when solving Eqs. (5) and (6). In this case we do not need to extrapolate the charged fraction to smaller sizes, which could affect the determined value of GR.

2.2.3 Advantages over previous methods

In the determination of the growth rate, the two methods described above have two advantages over previous methods that are based on following the centre of the nucleation mode (Lehtinen et al., 2003; Dal Maso et al., 2005; Hirsikko et al., 2005). Firstly, these methods are not restricted to any specific shape of the particle number size distribution. Secondly, these methods can, in principle, be used on charged fractions observed at any moment of time instead of needing a time series of observations. This has two advantages: (1) the growth rate can be determined as a function of time, as was done by Iida et al. (2008), and (2) the requirements for homogeneity of the measured air masses are not as strict as in the case of following the mode over a longer time period. When following the centre of a mode, it is assumed that the conditions in the air masses measured over a time period have been similar. Now, when analyzing data of a single moment of time, we only have to assume that the conditions in the measured air parcel have not varied too much, but similarity between consecutive moments of time is not needed.

3 Simulations and data analysis

3.1 The model

In this study, we used the aerosol dynamical box model Ion-UHMA (University of Helsinki Multicomponent Aerosol model for neutral and charged particles) which simulates the dynamical processes governing the time evolution of an aerosol particle size distribution (Leppä et al., 2009). The model divides aerosol particles into a user-specified number of size sections and three charge classes: electrically neutral and negatively- or positively-charged particles. All the charged particles are assumed to be singly-charged. Besides particles, there are pools of negative and positive small ions in the model. The small ions represent large molecules or molecular clusters with diameter < 1.8 nm. The electrical mobility of negative (positive) small ions is assumed to be 1.60 (1.40) $\mathrm{cm^2\ V^{-1}\ s^{-1}}$ which corresponds to diameter of ~ 1.16 (~ 1.24) nm (Ehn et al., 2011). The main processes simulated in Ion-UHMA are condensation of vapours onto particle surfaces, coagulation of particles and attachment of small ions to particles.

In this study, we did not simulate the condensation process, but the condensational growth rate of particle diameter was used as an input in the model. The growth scenarios used in the simulations will be described in more detail in Sects. 3.2.1–3.2.5. Also, the actual nucleation process was not simulated in the model, but the formation rate of particles was used as an input in the model. With this approach, we were not restricted to any nucleation theory or mechanism.

3.2 Simulation setup and parameters

A series of simulations was conducted with the following parameters varied: the new particle formation rate, particle diameter growth rate, fractions of particles formed carrying a negative or positive charge, and number concentration of larger pre-existing particles (Table 1).

In each simulation, the simulated particle diameter range was from 1.8 to 20 nm which was covered by 79 size sections spread evenly on a logarithmic scale. Additionally, the pre-existing population of larger particles was modelled by a single size section of 150-nm particles. The concentration of 150-nm particles was chosen to give the desired value of condensation sink (CS) that was kept constant during the simulation. In all simulations, the concentrations of negatively- and positively-charged small ions were 600 and 800 $\mathrm{cm^{-3}}$, respectively. The values of small ion concentrations were chosen to be similar to those observed in various measurements (Hirsikko et al., 2011). The duration of new particle formation was 4 h and the particles were assumed to be formed at $d_0 = 1.8$ nm. The new particle formation rate followed a sinusoidal pattern with the mean total formation rate presented in Table 1.

The values of condensation sink in the simulations varied from 0 to $1 \times 10^{-2}\ \mathrm{s^{-1}}$, which covers most of the observed values of condensation sink during new particle formation events in continental background areas (Birmili et al., 2003; Held et al., 2004; Dal Maso et al., 2007). The formation rate of particles varied from 0.0001 to 10 $\mathrm{cm^{-3}\ s^{-1}}$. The smallest value of formation rate used in the simulations would not be high enough to produce a new particle formation event observable with the current instrumentation. However, there is no such restriction for the model, and with such a small formation rate we can be sure that the amount of self-coagulation occurring in the simulation is negligible. New particle formation rates higher than the largest value used in the simulations have been observed in the measurements (e.g. Mönkkönen et al., 2005; Iida et al., 2008), but in such conditions, the coagulation processes are not taken into account sufficiently well in the analysis methods used in this study.

The six combinations of fractions of IIN were chosen to include the extreme cases of purely neutral and purely

Table 1. The values of parameters used as input in the model.

Parameter	Values used as input in the model
Particle diameter growth rate (nm h^{-1})	1; 3; 6; 10
New particle formation rate (cm^{-3} s^{-1})	0.0001; 0.1; 1; 3; 10
Concentration of 150-nm particles (cm^{-3})	0; 320; 960; 3200
Corresponding condensation sink (s^{-1})	0; 1×10^{-3}; 3×10^{-3}; 1×10^{-2}
Percentage of negative and positive ion-induced nucleation (%)	0&0; 5&5; 50&50; 3&0; 10&0.5; 40&10

Table 2. Summary of the growth rate scenarios described in Sects. 3.2.1–3.2.5.

Scenario	GR of neutral particles	GR of charged particles
1	$GR^0(d_p) = GR_{input}$	$GR^{\pm}(d_p) = GR_{input}$
2	$GR^0(d_p) = GR_{input}$	$GR^{\pm}(d_p) = \xi_{LK} \times GR_{input}$
3	$GR^0(d_p) = GR_{input}$	$GR^{\pm}(d_p) = \xi_{NY} \times GR_{input}$
4	$GR^0(d_p) = \tanh(0.2 \times d_p) \times GR_{input}$	$GR^{\pm}(d_p) = \tanh(0.2 \times d_p) \times GR_{input}$
5	$GR^0(d_p) = (2\text{-}\tanh(0.2 \times d_p)) \times GR_{input}$	$GR^{\pm}(d_p) = (2\text{-}\tanh(0.2 \times d_p)) \times GR_{input}$

ion-induced nucleation and a few cases around the values observed in field measurements (Laakso et al., 2007a; Manninen et al., 2010). The possible sign preference in IIN was also included as the fractions of particles formed carrying a negative and positive charge were not the same in all combinations.

Each combination of the input parameters was simulated with five different growth rate setups. The setups are described below and summarized in Table 2.

3.2.1 Growth rate scenario 1

In the first set up, the growth rate was constant as a function of the diameter and the same for neutral and charged particles, GR^0 and $GR^{\pm}$, respectively. The value of the growth rate was given as an input in the model, i.e. $GR^0 = GR^{\pm} = GR_{input}$. This setup is later denoted as growth rate scenario 1 (Fig. 1).

3.2.2 Growth rate scenario 2

In the second set up, GR^0 was constant as a function of the diameter, but $GR^{\pm}$ was multiplied by the diameter dependent enhancement factor, ξ_{LK}, (Lushnikov and Kulmala, 2004):

$$\xi_{LK}\left(d_p\right) = 1 + \frac{1}{4\pi\varepsilon_0}\frac{4e^2 r}{kT\left(d_p\right)^2}, \quad (7)$$

where ε_0 is the vacuum permittivity (8.85×10^{-12} F m^{-1}), e is the elementary charge (1.60×10^{-19} C), d_p is the particle diameter in meters, k is the Boltzmann constant (1.38×10^{-23} J K^{-1}) and T is the temperature in Kelvin. A polar molecule can be formally described as a compound having a negative and positive charge set apart by a fixed distance. This distance (in meters) is denoted by r in Eq. (7), with a value corresponding to sulphuric acid molecule used in this study. The value of the growth rate used as input in the model describes the growth rate of neutral particles, $GR^0 = GR_{input}$, and the growth rate of charged particles is given by $GR^{\pm} = \xi_{LK} \times GR_{input}$. $\xi_{LK}(d_p)$ is depicted in Fig. 1 (right panel) and this setup is later denoted as growth rate scenario 2.

3.2.3 Growth rate scenario 3

The third set up is the same as the second, except that the enhancement factor is given by (Nadykto and Yu, 2003)

$$\xi_{NY}\left(d_p\right) = 1 + \left(2 l_{SA} E\left(\frac{e^z + e^{-z}}{e^z - e^{-z}} - \frac{1}{z}\right) + a_{SA}\varepsilon_0 E^2\right) \Big/ \left(3kT\right), \quad (8)$$

where

$$z = \frac{l_{SA} E}{kT} \quad (9)$$

and

$$E = \left(\frac{1}{\varepsilon_g} - \frac{1}{\varepsilon_p}\right) \times \left(\frac{qe}{4\pi\varepsilon_0\left(r_{SA} + 0.5 d_p\right)^2}\right). \quad (10)$$

Here l_{SA} is the dipole moment of sulphuric acid (9.47×10^{-30} C m), a_{SA} is the polarizability of sulphuric acid (6.2×10^{-30} m^3), ε_g is the relative permittivity of vapour (~ 1.00 for air), ε_p is the relative permittivity of the particle (~ 100 for bulk sulphuric acid at temperature of 298 K) and q is the number of charges in the particle. $\xi_{NY}(d_p)$ is depicted in Fig. 1 (right panel) and this setup is later denoted as growth rate scenario 3.

3.2.4 Growth rate scenario 4

In the fourth setup, the growth rate of neutral and charged particles was the same and the growth rate increased as a

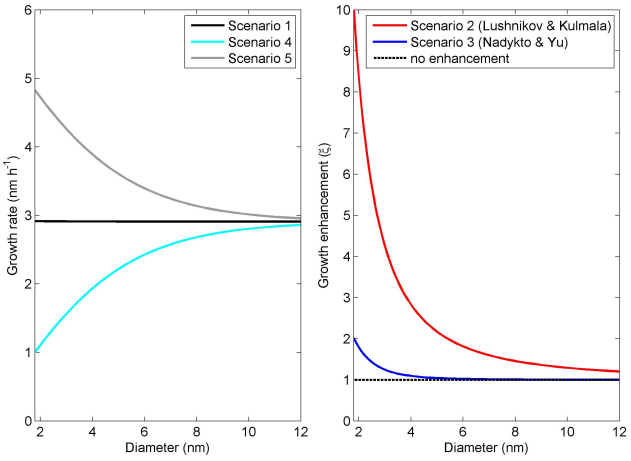

Fig. 1. Left panel: the particle diameter growth rates in the simulations with the same growth rate for neutral and charged particles (scenarios 1, 4 and 5). Only simulations with the value of $GR_{input} = 3\,nm\,h^{-1}$ are shown here, but the general shape as a function of diameter is similar for other values of GR_{input}. Right panel: the growth enhancement factor of charged particles in the simulations in which the growth rates of neutral and charged particles were different (scenarios 2 and 3). The black dashed line denotes unity, i.e. no enhancement of the growth rate.

function of the diameter according to

$$GR^0 = GR^{\pm} = \tanh\left(0.2 d_p\right) \times GR_{input} \quad (11)$$

where d_p is given in nanometres. The diameter dependence of the growth rate presented in Eq. (11) is arbitrarily chosen, but it is similar to the diameter dependence observed in field measurements (Hirsikko et al., 2005; Yli-Juuti et al., 2011; Kuang et al., 2012). Growth rates with this setup for $GR_{input} = 3\,nm\,h^{-1}$ are depicted in Fig. 1 (left panel) and this setup is later denoted as growth rate scenario 4.

3.2.5 Growth rate scenario 5

In the fifth setup, the growth rate of neutral and charged particles was the same and the growth rate decreased as a function of diameter according to

$$GR^0 = GR^{\pm} = \left(2 - \tanh\left(0.2 d_p\right)\right) \times GR_{input} \quad (12)$$

where d_p is given in nanometres. The diameter dependence of the growth rate presented in Eq. (12) is arbitrarily chosen, but it is similar to the diameter dependence of the theoretical condensational growth rate by sulphuric acid (Nieminen et al., 2010). Growth rates with this setup for $GR_{input} = 3\,nm\,h^{-1}$ are depicted in Fig. 1 (left panel) and this setup is later denoted as growth rate scenario 5.

3.3 Analysis of the simulated data

The model provided the charging states, $S^{\pm}$, and the charged fractions, $f^{\pm}$, both as a function of time and diameter. In order to simplify the analysis, we used only one value of $S^{\pm}$ and $f^{\pm}$ at each diameter, instead of allowing it to vary in time. For each size section, the values of $S^{\pm}$ and $f^{\pm}$ used in the analysis were taken at the moment of highest particle concentration at that size section, i.e. the values of $S^{\pm}$ and $f^{\pm}$ were taken along the trajectory of the centre of the mode. Furthermore, instead of using the whole resolution of the model, we interpolated the values of $S^{\pm}$ and $f^{\pm}$ to a more coarse resolution (2.2, 2.5, 3.0, 3.9, 5.1, 6.7, 8.8 and 11.5 nm), which was chosen to match the resolution of Ion-DMPS system as described by Gagné et al. (2012). These simulated data points were then used to determine the growth rate and initial fraction of charged particles in a similar way as measured data points were used by Gagné et al. (2012). This was done in order to provide results that are relevant from the atmospheric measurements point of view.

When analyzing the growth rate and initial charged fractions, we used the following two diameter ranges: from 2.2 to 11.5 nm (2.2, 2.5, 3.0, 3.9, 5.1, 6.7, 8.8 and 11.5 nm) and from 3.0 to 11.5 nm (3.0, 3.9, 5.1, 6.7, 8.8 and 11.5 nm), which will be denoted as diameter range 1 (DR 1) and 2 (DR 2), respectively. This was done to provide results that are useful from the point of view of field measurements, in which observations below 3 nm are not always available (e.g. Laakso et al., 2007a).

The condensational growth rates in the simulations, GR_{sim}, were ambiguous, since in the growth rate scenarios 2 and 3 charged particles grew more rapidly than the neutral ones, and also because in the scenarios 4 and 5 all the particles grew with a diameter-dependent rate. Furthermore, the division of the particles into the size sections in the model resulted in a small error in the condensational growth rate of the particles in all of the simulations (Leppä et al., 2011). Since the iteration and fitting methods provide two estimates on the value of GR for each simulation (one for DR 1 and the other for DR 2), we needed to estimate the corresponding values of GR_{sim} in order to compare the values determined with the methods to those observed in the simulations. When estimating the value of GR_{sim}, the growth rates of neutral and charged particles were weighted with the fractions of neutral and charged particles, respectively, and the effect of numerical error was estimated according to equations presented by Leppä et al. (2011). The values of GR_{sim} for DR 1 (DR 2) was then estimated to be the average growth rate of the particles during their growth from 2.2 (3.0) to 11.5 nm in diameter. As a result, we obtained two values of the growth rate for every simulation: one to be compared to the estimated growth rates obtained using data points in DR 1 and the other to be compared to the estimated growth rates obtained using DR 2.

An estimate of the particle diameter growth rate was determined in 12 different ways from every simulation. Eight of them were obtained using the iteration method, with all combinations of the following three options used: (1) either DR 1 or DR 2 was used; (2) the small ion concentrations were either 600 and 800 cm^{-3} for negative and positive

ions, respectively, or both concentrations were assumed to be 700 cm^{-3}; (3) when solving Eqs. (5) and (6), the starting diameter was either 1.8 nm or the smallest diameter of the data points (2.2 or 3.0 nm). In this study, the small ion concentrations of 600 and 800 cm^{-3} for negative and positive ions, respectively, will be denoted as asymmetric small ion concentrations and the concentrations of 700 cm^{-3} for both polarities will be denoted as symmetric small ion concentrations. Four estimates of the growth rate were obtained using the fitting method with separate growth rates obtained from the fits to negative and positive charging states and with either DR 1 or DR 2 used for the fittings.

4 Results

4.1 Charged fraction, formation rate and ion-induced nucleation

The simulated fraction of charged particles at 1.8 nm was not the same as the fraction of particles formed carrying a charge ($IIN^{\pm}$). The formation of the particles was a source term of the particles at 1.8 nm, but the charged fraction depends on the concentrations of the neutral and charged particles, for which the sink terms had to be taken into account. Since the fitting and iteration methods provided estimates on the initial charged fraction, the values obtained using those methods were compared with the values of the charged fraction at 1.8 nm in diameter obtained directly from the simulations. However, since the initial charged fraction and the proportion of IIN have been assumed to be equal in previous studies (Laakso et al., 2007a; Gagné et al., 2008, 2010, 2012), we also compared the initial charged fractions determined with the methods to the proportions of IIN used as input in the model (Appendix A).

In the simulations, the removal rates of charged particles due to self-coagulation and coagulation scavenging were larger than the corresponding removal rates of neutral particles, so the charged fractions were smaller than the corresponding fractions of $IIN^{\pm}$ (Fig. 2). If the concentrations of nucleation-mode and pre-existing particles were small, the coagulation processes were negligible and, thus, the ratio of the $f_{\mathrm{ini}}^{\pm}$ to the corresponding fraction of $IIN^{\pm}$ was close to unity, provided that the charged particles grew by the same rate as the neutral ones. However, if the coagulation processes were significant, the ratio of the $f_{\mathrm{ini}}^{\pm}$ to the fraction of $IIN^{\pm}$ was as low as ~ 0.5, which means that estimating the fraction of $IIN^{\pm}$ from the initial charged fraction could lead to an underestimation of $IIN^{\pm}$ by up to a factor of 2.

Furthermore, if charged particles grew more rapidly than neutral ones, the ratio of $f_{\mathrm{ini}}^{\pm}$ to the fraction of $IIN^{\pm}$ was ~ 0.4–0.7 and < 0.05 for simulations with moderate (GR scenario 3) and large (GR scenario 2) growth enhancement, respectively, unless all particles were formed carrying a charge. This was due to the higher removal rate of charged

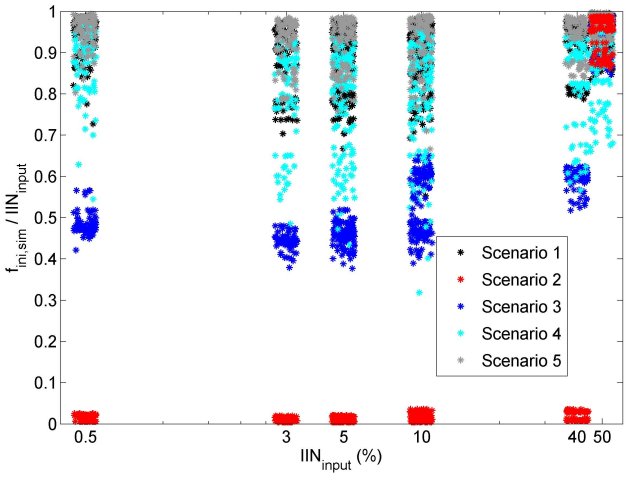

Fig. 2. The ratio of the simulated (negative or positive) charged fraction at 1.8 nm and the fraction of (negative or positive) ion-induced nucleation used as input in the model as a function of the fraction of (negative or positive) ion-induced nucleation. The colours denote the growth scenario used in the simulation as indicated in the legend. A random variation of up to 10 % is added to the values on the x-axis to make data points more distinguishable. The data points from the simulations with 0 % of ion-induced nucleation are excluded from the figure.

than neutral 1.8-nm particles, which resulted from the growth rate of charged particles being higher than that of neutral ones. The role of the enhanced growth of charged particles in relation to $IIN^{\pm}$ and the particle size distribution can be demonstrated by writing the flux of particles through diameter d_0, i.e. the apparent formation rate at d_0, as $J^q(d_0) = \mathrm{GR}^q(d_0) \times n^q(d_0)$, where q is the charge of the particle and n^q is the particle size distribution ($n^q = \mathrm{d}N^q/\mathrm{d}d_{\mathrm{p}}$). Now, the $IIN^{\pm}$ can be written as

$$IIN^{\pm} = \frac{J_0^{\pm}}{J_0^{\mathrm{tot}}} = \frac{\mathrm{GR}_0^{\pm} n_0^{\pm}}{\mathrm{GR}_0^0 n_0^0 + \mathrm{GR}_0^{\pm} n_0^- + \mathrm{GR}_0^{\pm} n_0^+} = \frac{\xi n_0^{\pm}}{n_0^0 + \xi\left(n_0^- + n_0^+\right)} \quad (13)$$

where ξ is the enhancement factor ($\mathrm{GR}^{\pm} = \xi \times \mathrm{GR}^0$) and 0 in the lower index denotes that the value is taken at the size d_0. If all particles were formed carrying a charge, then all particles grew by this increased rate, in which case there was no difference in the removal rate of charged and neutral particles. Thus, the ratio of $f_{\mathrm{ini}}^{\pm}$ to the corresponding fraction of $IIN^{\pm}$ was close to unity.

It should be noted that the values shown in Fig. 2 correspond to the simulations with the formation size of 1.8 nm in diameter. The removal processes causing the difference between $f_{\mathrm{ini}}^{\pm}$ and the corresponding fraction of $IIN^{\pm}$ are diameter dependent and, thus, the results would be different for different formation sizes. Examples of such differences will be given in Sect. 4.2.2.

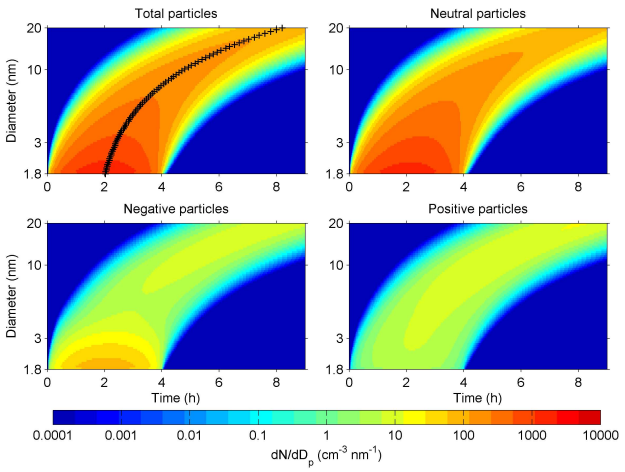

Fig. 3. The time evolution of the particle number size distribution from the example simulation described in Sect. 4.2. The black crosses mark the centre of the mode.

4.2 An example case

The time evolution of the particle size distribution for an example simulation is depicted in Fig. 3. In this simulation, the new particle formation rate, particle diameter growth rate and concentration of larger pre-existing particles used as input in the model were 1 cm^{-3} s^{-1}, 3 nm h^{-1} and 960 cm^{-3}, respectively. The growth rate scenario 3 was used in this simulation and the fractions of particles formed carrying negative and positive charge were 10 and 0.5 %, respectively. By looking at the value of the particle number size distribution at the centre of the nucleation mode, we see that the total concentration decreased with an increasing particle diameter, which is due to coagulation losses. The concentration of positive particles increased with increasing diameter because of the higher charging probability. The concentration of negative particles first decreased and then started to increase with an increasing diameter. This resulted from the large fraction of particles formed carrying a negative charge, which was larger than the fraction of negatively-charged particles in the charge equilibrium.

The negative and positive charging states, S^- and S^+, changed as a function of time and diameter (Fig. 4). Both negative and positive charging states were the highest at the very beginning of the new particle formation event. In this case, the high values of S at the beginning were due to a higher growth rate of charged particles (GR scenario 3), as fewer neutral than charged particles had had time to grow to larger sizes. The strong time dependence of S disappeared gradually, making S to be mainly dependent on the particle diameter.

The negatively-charged fraction at 1.8 nm estimated using the iteration method decreased to less than half when the diameter range 1 was used instead of the diameter range 2 (Fig. 4). A similar decrease in the negative charging state at 1.8 nm estimated using the fitting method was also observed.

The fitting method assumed that the change rates of the charged fractions are dominated by the ion-aerosol attachment and intramodal recombination, whereas the iteration method assumed that the change rates are dominated only by ion-aerosol attachment. The fractions of change rates of the negative and positive charged fractions taken into account in the fitting (iteration) method, F_{fit} (F_{iter}), were ~ 0.87 (~ 0.86) and ~ 0.90 (~ 0.84), respectively, which means that the dominating processes were taken into account by these methods. The difference in the values of F_{fit} and F_{iter} was larger for values determined from positive than negative polarity, which means that the intramodal recombination was relatively more important process changing the fraction of positive than negative particles. The procedure that has been used to estimate the fractions of change rates of charged fractions taken into account in the iteration and the fitting methods is described in detail in Appendix B.

4.2.1 Particle growth rates in the example case

The 12 estimates of the growth rate determined using the iteration and fitting methods (see Sect. 3.3.1) were compared with the simulated condensational growth rate, $\mathrm{GR_{sim}}$. In our example case, the values of $\mathrm{GR_{sim}}$ averaged over DR 1 and DR 2 were 2.92 and 2.93 nm h^{-1}, respectively (Table 3), while the value of growth rate used as input in the model, $\mathrm{GR_{input}}$, was 3.0 nm h^{-1}. The values of $\mathrm{GR_{sim}}$ were smaller than the value of $\mathrm{GR_{input}}$ due to numerical errors caused by the division of particles to the fixed sections in the model. This difference was partly compensated by the enhanced condensation onto charged particles.

The values of $\mathrm{GR_{iter}}$ are shown in Table 3. The starting diameter used when solving Eqs. (5) and (6) had very little effect on the $\mathrm{GR_{iter}}$ in this case, and whether we used the asymmetric or symmetric small ion concentrations had a considerable effect on the $\mathrm{GR_{iter}}$. However, whether we used DR 1 or DR 2 also had a considerable effect on the $\mathrm{GR_{iter}}$. This was due to the combination of a considerable proportion of IIN (10 % and 0.5 % for negative and positive particles, respectively), and due to the fact that the charged particles grew more rapidly than the neutral ones (GR scenario 3). For the same reason, there was a difference in the results between DR 1 and DR 2, as the growth enhancement of the charged particles was diameter dependent.

The values of $\mathrm{GR^-_{fit}}$ ($\mathrm{GR^+_{fit}}$) were larger (smaller) than the corresponding values of $\mathrm{GR_{sim}}$, especially for $\mathrm{GR^-_{fit}}$ when DR 1 was used (Table 3). The reason for this was that charged particles grew more rapidly than neutral ones in the simulation (GR scenario 3), but this was not taken into account in the fitting method. The enhanced growth of charged particles resulted in smaller values of the charging state, especially in the small sizes, in which the enhancement was the largest. Since DR 1 covers smaller sizes than DR 2, the enhanced

Table 3. The values related to the example simulation described in Sect. 4.2. The starting diameter used when solving Eqs. (5) and (6) is denoted as $d_{\mathrm{p,ini}}$. DR 1 and DR 2 denote the diameter ranges 1 (2.2–11.5 nm) and 2 (3–11.5 nm), respectively.

	GR (nm h^{-1})	IIN^-/f_{ini}^- (%)	IIN^+/f_{ini}^+ (%)
Model input	3	10	0.5
Simulation, DR 1 (DR 2)	2.93 (2.92)	4.65	0.245
Fitting method on negative S, DR 1	4.48	6.59	–
Fitting method on negative S, DR 2	3.11	10.6	–
Fitting method on positive S, DR 1	2.57	–	0.287
Fitting method on positive S, DR 2	2.67	–	0.396
Iteration method with asymmetric small ions, DR 1, $d_{\mathrm{p,ini}} = 1.8$ nm ($d_{\mathrm{p,ini}} = 2.2$ nm)	4.93 (4.93)	7.90	0.610
Iteration method with asymmetric small ions, DR 2, $d_{\mathrm{p,ini}} = 1.8$ nm ($d_{\mathrm{p,ini}} = 3.0$ nm)	3.38 (3.34)	17.7	1.12
Iteration method with symmetric small ions, DR 1, $d_{\mathrm{p,ini}} = 1.8$ nm ($d_{\mathrm{p,ini}} = 2.2$ nm)	4.48 (4.49)	7.45	0.818
Iteration method with symmetric small ions, DR 2, $d_{\mathrm{p,ini}} = 1.8$ nm ($d_{\mathrm{p,ini}} = 3.0$ nm)	4.34 (4.35)	7.83	2.80

growth of charged particles had more effect on the growth rate determined with the fitting method when DR 1 was used instead of DR 2 and this effect was larger for GR_{fit}^- than for GR_{fit}^+ because of the higher negative than positive charging state.

The value of GR_{fit}^- was $\sim 74\,\%$ ($\sim 16\,\%$) larger than the value of GR_{fit}^+, if the data from DR 1 (DR 2) was used in the fitting method (Table 3). The considerable difference between the values of GR_{fit}^- and GR_{fit}^+ when DR 1 was used was due to enhanced growth rate of charged particles (GR scenario 3) in the simulation, which was not taken into account in the fitting method.

4.2.2 The initial charged fractions in the example case

In our example simulation, the fractions of negative and positive IIN were 10 and 0.5 %, respectively, whereas the values of $f_{\mathrm{ini,sim}}^-$ and $f_{\mathrm{ini,sim}}^+$ were ~ 4.7 and $\sim 0.25\,\%$, respectively (Table 3). The observed difference of a factor of two between the input fraction of IIN and the simulated value of initial charged fraction was a very typical result for a simulation using the growth rate scenario 3. However, if the formation size of the particles had been 1.5 (1.2) nm instead of 1.8 nm, the values of $f_{\mathrm{ini,sim}}^-$ and $f_{\mathrm{ini,sim}}^+$ would have been ~ 3.6 (~ 2.4) and ~ 0.18 (~ 0.12), respectively. In other words, the difference of a factor of almost three or slightly above four between the input fraction of IIN and the simulated value of initial charged fraction would have been observed, if the particles had been formed at 1.5 or 1.2 nm in diameter, respectively. This means that the formation size affects the difference between the simulated initial charged fraction and the fraction of IIN used as input in the model.

The values of $f_{\mathrm{ini,fit}}^-$ and $f_{\mathrm{ini,fit}}^+$, were 6.6 and 0.29 %, respectively, when DR 1 was used; and 11 and 0.40 %, respectively, when DR 2 was used (Table 3). Since the values of $f_{\mathrm{ini,sim}}^-$ and $f_{\mathrm{ini,sim}}^+$ were 4.7 and 0.25 %, respectively, the fitting method was able to approximately reproduce the simulated value, when DR 1 was used, but overestimated the initial charged fraction, if DR 2 was used.

The values of $f_{\mathrm{ini,iter}}^-$ and $f_{\mathrm{ini,iter}}^+$, were 7.9 (7.4) and 0.61 % (0.82 %), respectively, when DR 1 and the asymmetric (symmetric) small ion concentrations were used and 18 (7.8) and 1.1 % (2.8 %), respectively, when DR 2 and asymmetric (symmetric) small ion concentrations were used (Table 3). Since the values of $f_{\mathrm{ini,sim}}^-$ and $f_{\mathrm{ini,sim}}^+$ were 4.7 and 0.25 %, respectively, the iteration method overestimated both the negative and the positive initial charged fraction. However, this overestimation was smaller when DR 1 was used instead of DR 2, especially when asymmetric small ion concentrations were used.

4.3 Determination of the growth rate

The analysis described in Sect. 3.3 was conducted for every simulation in the simulation set described in Sect. 3.2. Here we will present the results of the comparison of the determined and the simulated growth rates for the whole simulation set.

4.3.1 The growth rate determined with the iteration method

The growth rates estimated using the iteration method with asymmetric small ion concentrations, $GR_{\mathrm{iter,asy}}$, using data points in DR 2 and by solving Eqs. (5) and (6) starting from the size 1.8 nm are shown in Fig. 5. The iteration method used here assumes that the changes in the fraction of charged particles are dominated by the ion-aerosol attachment, which is not the case in all the simulations. In the cases where the changes were dominated by ion-aerosol attachment, the correspondence between $GR_{\mathrm{iter,asy}}$ and GR_{sim} was good, except in the simulations with the growth rate scenario 2. In that scenario charged particles grew much more rapidly than neutral ones, but in the iteration method it is assumed that all the particles grow by the same rate regardless of their charge. In the simulations with other growth rate scenarios, $GR_{\mathrm{iter,asy}}$ tended to be larger than GR_{sim}, especially if GR_{sim}

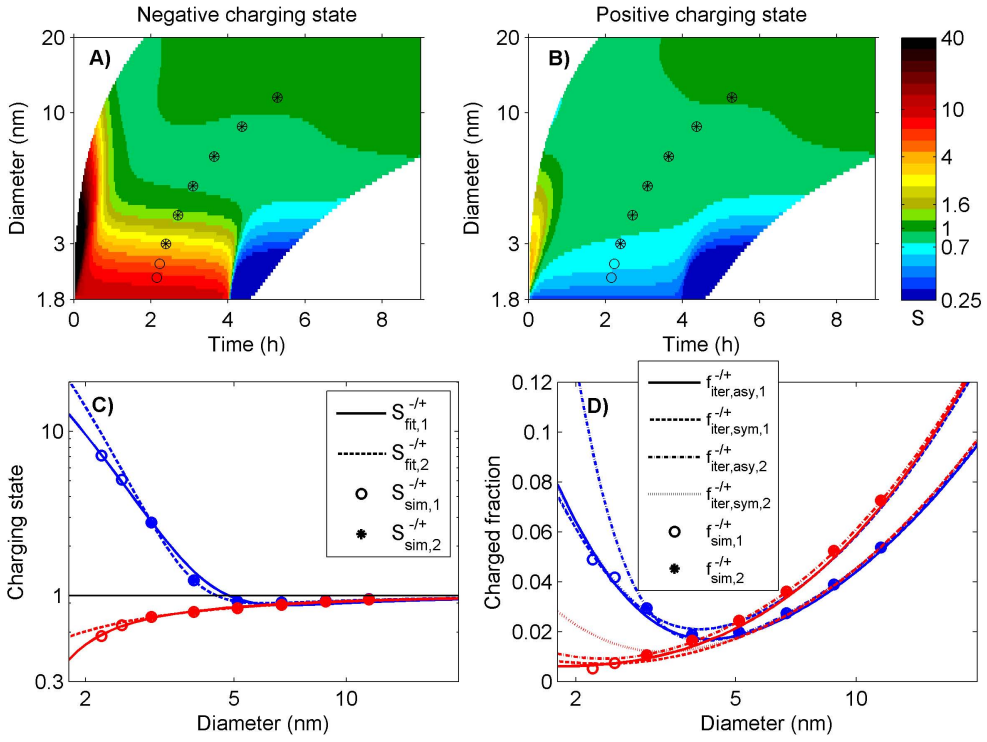

Fig. 4. The upper panels depict the aerosol charging state of the example simulation as a function of time and diameter with the colours representing the value of the negative **(A)** and the positive **(B)** charging state. The lower panels depict the charging state **(C)** and the charged fraction **(D)** as a function of diameter obtained by following the centre of the mode. In the lower panels, the blue and red colours indicate the negative and the positive charging state or charged fraction, respectively. The circles denote the simulated values and the lines denote the iterated **(C)** or the fitted **(D)** values. In the legends, "asy" and "sym" denote whether asymmetric or symmetric small ion concentrations have been used, respectively, and numbers 1 and 2 indicate whether the data from DR 1 (2.2–11.5 nm) or DR 2 (3–11.5 nm), respectively, had been used. In **(D)**, in the sizes > 5 nm, the upper (lower) group of lines almost on top of each other include the lines denoting $f^{-}_{\mathrm{iter,sym}}$ and $f^{+}_{\mathrm{iter,asy}}$ ($f^{-}_{\mathrm{iter,asy}}$ and $f^{+}_{\mathrm{iter,sym}}$). In **(D)**, in the sizes < 5 nm, the upmost blue line denotes the $f^{-}_{\mathrm{iter,asy,1}}$, whereas the other three blue lines are almost on top of each other.

was small, but in a majority of cases, the difference between $\mathrm{GR_{iter,asy}}$ and $\mathrm{GR_{sim}}$ was small.

The results presented above were obtained by using the iteration method with asymmetric small ion concentrations with the data points taken from DR 2 and by solving Eqs. (5) and (6) starting from the size 1.8 nm. We also determined the growth rate by using the iteration method with symmetric small ion concentrations, by using data points from diameter range 1 and by solving Eqs. (5) and (6) starting from the smallest size of the diameter range of the data points (2.2 or 3.0 nm). We found that $\mathrm{GR_{iter}}$ was not very sensitive to the used diameter range nor to the starting diameter used when solving Eqs. (5) and (6). However, whether we used the asymmetric or symmetric small ion concentrations did have a significant effect on $\mathrm{GR_{iter}}$, especially if $\mathrm{GR_{sim}}$ was small (Fig. 5). When $\mathrm{GR_{sim}}$ was small, the charged fractions approached the charge equilibrium rapidly, regardless of the initial charged fraction. The equilibrium charged fractions depend on small ion concentrations, which were asymmetric in the simulation, but assumed to be either asymmetric or symmetric when using the iteration method. Now, when using symmetric small ion concentrations in the iteration method, the equilibrium charged fractions assumed in the iteration were different to those in the simulation. In such cases, the method overestimated the growth rate in order to reduce the discrepancy between the simulated charged fractions and those obtained by solving Eqs. (5) and (6).

4.3.2 The growth rate determined with the fitting method

The growth rates obtained using the fitting method on the negative charging state, $\mathrm{GR^{-}_{fit}}$, are shown in Fig. 6. The fitting method assumed that the changes in the charged fraction were dominated by ion-aerosol attachment and the recombination within the nucleation mode, which was a good assumption for the vast majority of the simulations. However, the correspondence between $\mathrm{GR_{sim}}$ and $\mathrm{GR^{-}_{fit}}$ was bad for the simulations with growth rate scenario 2, when DR 2 was used. Also, there were more cases with $\mathrm{GR^{-}_{fit}}$ overestimating

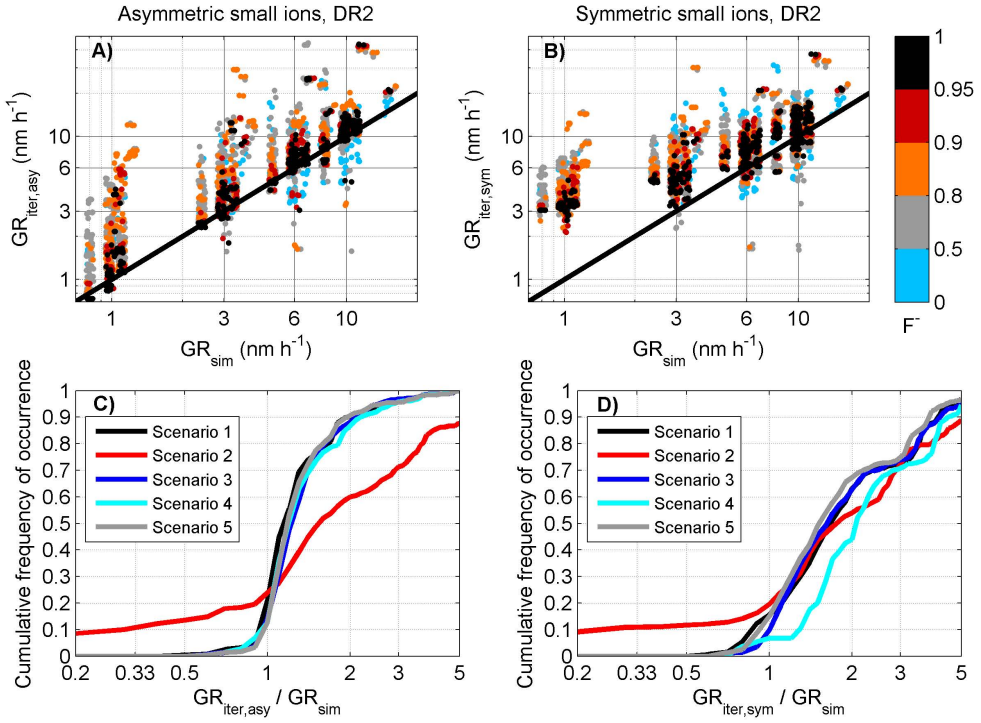

Fig. 5. Upper panels: the particle diameter growth rate determined using the iteration method as a function of the growth rate in the simulation. The colour indicates the fraction of the change rate of the charged fraction, F^-, that was taken into account in the method (details in Appendix B). Lower panels: the cumulative frequency of occurrence of the ratio of the determined growth rate to the growth rate in the simulation. Different lines denote the simulations with different growth rate scenarios as indicated in the legend. The panels on the left (**A** and **C**) and the right hand side (**B** and **D**) denote the results obtained using asymmetric and symmetric small ion concentrations, respectively, with DR 2 (3–11.5 nm).

GR_{sim} than underestimating it, especially if GR_{sim} was small. Overall, the correspondence between GR_{fit}^{-} and GR_{sim} for growth rate scenarios other than 2 was moderate, when DR 2 was used.

If DR 1 was used, however, the correspondence between GR_{fit}^{-} and GR_{sim} was poor, especially for the simulations with growth rate scenario 2, and the correspondence behaved differently for the simulations using different growth rate scenarios (Fig. 6). The difference in the results obtained using either DR 1 or DR 2 was most evident in the case of growth rate scenario 4, for which the underestimation of the GR_{sim} was much more frequent when DR 1 was used instead of DR 2. Only results for the fits to negative charging states are given here, but the corresponding results for the fits to positive charging states were very similar.

The reason for the worse correspondence between GR_{fit}^{-} and GR_{sim} when DR 1 was used instead of DR 2 was that some of the assumptions made in the fitting method were less appropriate for that range. Firstly, in the fitting method it was assumed that all the particles grew by the same rate regardless of their size or the charge they carried. This should not, however, be enough to explain the difference between the results related to the two size ranges, since the same assumptions were made in the iteration method, for which there was very little difference between the results related to the different diameter ranges. Secondly, in the fitting method, the ion-aerosol attachment coefficient was assumed to increase linearly as a function of particle diameter and the recombination coefficient between a small ion or charged particle with an oppositely-charged particle was assumed to be constant as a function of diameter (Kerminen et al., 2007). Neither of these two assumptions held exactly in the simulations. These assumptions were good for a very narrow diameter range, but they got worse as the diameter range got wider.

4.4 Determination of the initial charged fraction

The initial charged fractions determined with the fitting and iteration methods ($f_{ini,fit}^{\pm}$ and $f_{ini,iter}^{\pm}$, respectively) were compared to the simulated initial fractions, $f_{ini,sim}^{\pm}$. The results were divided into the following three categories: (1) both $f_{ini,sim}^{\pm}$ and $f_{ini,fit}^{\pm}$ or $f_{ini,iter}^{\pm} < 1\,\%$; (2) $f_{ini,sim}^{\pm} < 1\,\%$, but $f_{ini,fit}^{\pm}$ or $f_{ini,iter}^{\pm} > 1\,\%$; (3) $f_{ini,sim}^{\pm} > 1\,\%$. The limit value of 1 % used to define the aforementioned categories was arbitrarily chosen to be a limit below which the fraction of charged particles was considered to be small. The

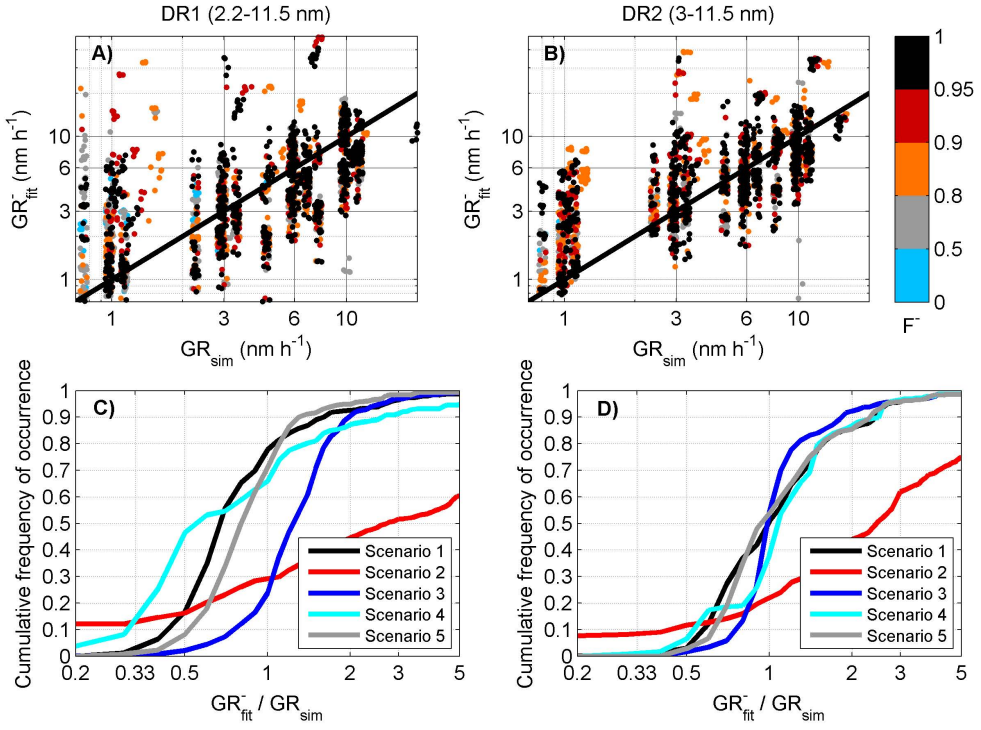

Fig. 6. Upper panels: the particle diameter growth rate determined using the fitting method as a function of the growth rate in the simulation. The colour indicates the fraction of the change rate of the negative charged fraction, F^-, that was taken into account in the method (details in Appendix B). Lower panels: the cumulative frequency of occurrence of the ratio of the determined growth rate to the growth rate in the simulation. Different lines denote the simulations with different growth rate scenarios as indicated in the legend. The panels on the left (**A** and **C**) and the right hand side (**B** and **D**) denote the results obtained using negative charging states from DR 1 (2.2–11.5 nm) and DR 2 (3–11.5 nm), respectively.

conclusions of this study would not change, if another value reasonably close to 1 % was chosen for this limit.

It then followed that the results in category 1 were considered to be good results, regardless of the occasionally high relative difference in the $f^{\pm}_{\mathrm{ini,sim}}$ and $f^{\pm}_{\mathrm{ini,fit}}$ or $f^{\pm}_{\mathrm{ini,iter}}$, since both of them were small. The results in category 2 were undesirable, since in those cases the simulated value was small, but the value obtained from the fitting or iteration method would indicate a considerable fraction of charged particles. Finally, the results in category 3 were most suitable for assessing how well the fitting or iteration method had been able to determine $f^{\pm}_{\mathrm{ini,sim}}$, and therefore the correspondence between $f^{\pm}_{\mathrm{ini,sim}}$ and $f^{\pm}_{\mathrm{ini,fit}}$ or $f^{\pm}_{\mathrm{ini,iter}}$ for results in category 3 was studied in more detail.

4.4.1 The initial charged fraction determined with the iteration method

The initial negative charged fractions determined with the iteration method with asymmetric small ion concentrations, $f^{-}_{\mathrm{ini,iter}}$, as a function of corresponding charged fractions from the simulations, $f^{-}_{\mathrm{ini,sim}}$, are shown in Fig. 7. Regardless of whether the data points were from DR 1 or DR 2, there were results in all three categories. The vast majority of the results in the undesired category 2 were from the simulations in which $\mathrm{GR_{input}}$ was 1 nm h^{-1} and/or growth rate scenario 2 was used.

Let us now have a more detailed look at the results belonging to the category 3. If the data points were taken from DR 2, the correspondence between $f^{-}_{\mathrm{ini,iter}}$ and $f^{-}_{\mathrm{ini,sim}}$ for results in category 3 was poor (Fig. 7). When charged particles grew more rapidly than neutral ones (GR scenarios 2 and 3), the iteration method tended to overestimate $f^{-}_{\mathrm{ini,sim}}$ because the higher removal rate of charged than neutral particles due to the different growth rates was not taken into account. In other cases (GR scenarios 1, 4 and 5), the iteration method tended to underestimate $f^{-}_{\mathrm{ini,sim}}$. However, if the data points were taken from DR 1, the correspondence between $f^{-}_{\mathrm{ini,iter}}$ and $f^{-}_{\mathrm{ini,sim}}$ for the results in category 3 was good, except for the overestimation of $f^{-}_{\mathrm{ini,sim}}$ in the simulations in which GR scenario 2 or 3 was used and the underestimation of $f^{-}_{\mathrm{ini,sim}}$ in the simulations in which GR scenario 4 was used. The underestimation in case of GR scenario 4 was mainly because the method assumed that the growth rate was constant with particle size, causing overestimation of the growth rate in the

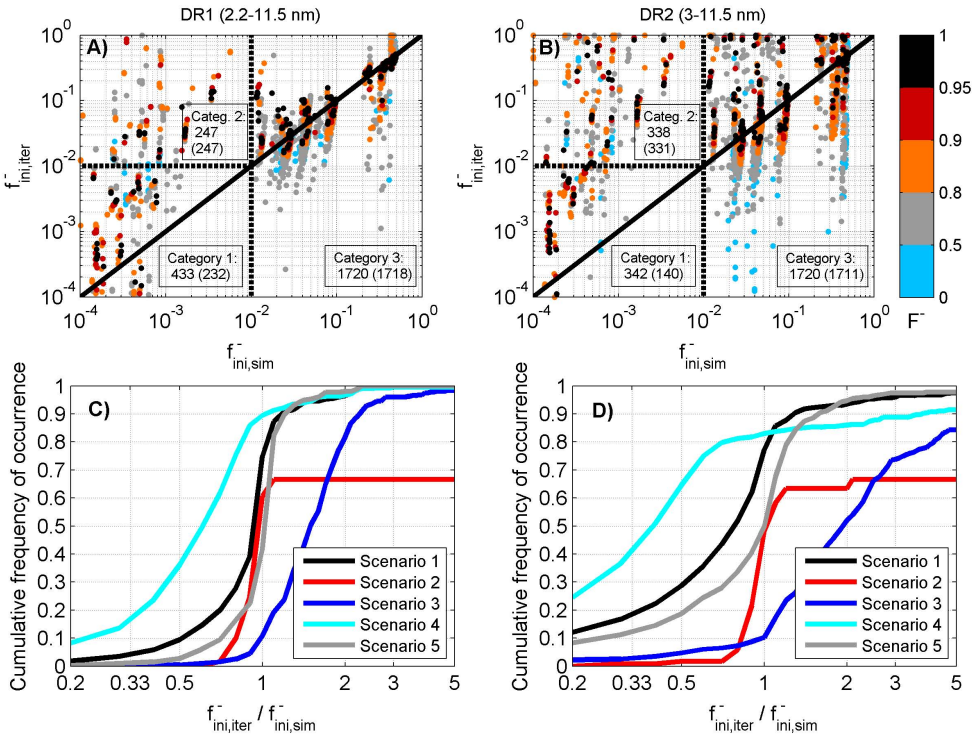

Fig. 7. The initial negative charged fractions determined with the iteration method using asymmetric small ion concentrations as a function of the initial charged fractions in the simulation are depicted in the upper panels for two diameter ranges. The colour denotes the fraction of the change rate of the negative charged fraction that was taken into account in the method (see details in Appendix B). The solid black line denotes the one to one correspondence and the dashed lines divide the data points into the 3 categories described in Sect. 4.4. The numbers denote the number of data points in each category with the numbers in parenthesis denoting the number of data points shown in the figure. The points not shown in the figure had either the value of $f^-_{\mathrm{ini,iter}}$ or $f^-_{\mathrm{ini,sim}} < 1 \times 10^{-4}$. The cumulative frequency of occurrence of the ratio of the fitted and the simulated initial charged fraction are depicted in lower panels with different colours denoting different growth scenarios used in the simulations. Only the data points in category 3 of **(A)** and **(B)** were used to obtain the curves in **(C)** and **(D)**, respectively. The panels on the left (**A** and **C**) and right hand side (**B** and **D**) denote the results obtained using data from DR 1 (2.2–11.5 nm) and DR 2 (3–11.5 nm), respectively.

small sizes. For this reason, the charged fraction approached the value in the charge equilibrium less rapidly in the method than in the simulation, which resulted in an underestimation of the initial charged fraction when $f^-_{\mathrm{ini,sim}}$ was higher than the corresponding value in the equilibrium. In the iteration method used in this study, it was assumed that the changes in the charged fraction were dominated by ion-aerosol attachment. However, this was not the case in many of the simulations. By excluding the simulations, in which less than $\sim$85 % of the changes in the charged fractions were due to ion-aerosol attachment, the correspondence between $f^-_{\mathrm{ini,iter}}$ and $f^-_{\mathrm{ini,sim}}$ became much better than with all simulations included. Furthermore, the correspondence between $f^-_{\mathrm{ini,iter}}$ and $f^-_{\mathrm{ini,sim}}$ was better in simulations with a high $\mathrm{GR_{input}}$, low formation rate and low condensation sink than in the simulations with a small $\mathrm{GR_{input}}$, high formation rate and high condensation sink. This was because the higher the growth rate is and the smaller the change rate of the charged fraction is, the longer the particle population bears memory of the initial charging state (Kerminen et al., 2007). In the simulations in which $\mathrm{GR_{input}}$ was 1 nm h^{-1}, the correspondence between $f^-_{\mathrm{ini,iter}}$ and $f^-_{\mathrm{ini,sim}}$ was much worse than in the simulation with higher values of $\mathrm{GR_{input}}$, as the information of the initial charged fraction was minimal at the diameter range of the data points. The results for $f^+_{\mathrm{ini,iter}}$ were very similar to the corresponding results for $f^-_{\mathrm{ini,iter}}$.

If the symmetric small ion concentrations were used when determining $f^-_{\mathrm{ini,iter}}$, the correspondence between $f^-_{\mathrm{ini,iter}}$ and $f^-_{\mathrm{ini,sim}}$ was worse than in the case of asymmetric small ion concentrations being used, especially when the data were taken from DR 2. The reason for this was that when assuming the symmetric small ion concentrations, the concentration of negative small ions was overestimated and the concentration of positive ions was underestimated. Thus, the negative charging of neutral particles was overestimated and the neutralization of negative particles was underestimated. Consequently, the initial negative charged fraction changed less rapidly than in the case of asymmetric small ion

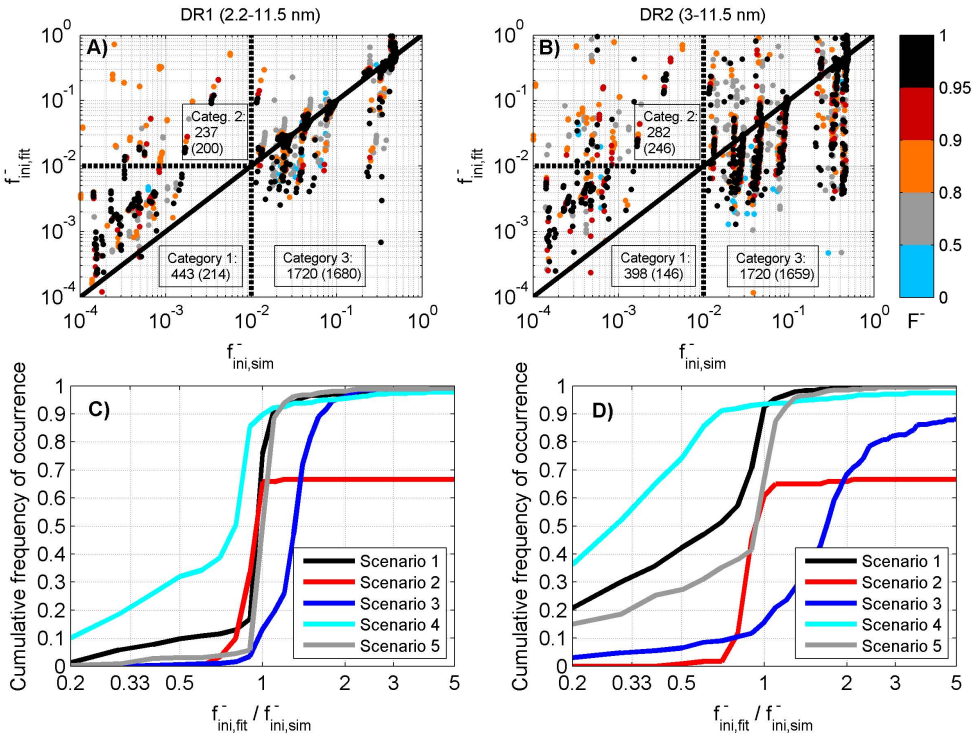

Fig. 8. As Fig. 7, except that the initial charged fractions on the y-axis of **(A)** and **(B)** are determined using the fitting method, instead of the iteration method, and the cumulative frequencies of occurrence shown in **(C)** and **(D)** are changed accordingly.

concentrations being assumed. For this reason, if the initial negative charged fraction in the simulation was overcharged, then a smaller initial negative charged fraction was needed in the iteration method to match the simulated values, which resulted in an underestimation of the initial negative charged fraction. If the data were taken from DR 1, the differences between the values of negative initial charged fractions iterated with asymmetric and symmetric small ion concentrations were smaller than in the case of DR 2. For $f^{+}_{\mathrm{ini,iter}}$, the situation was the opposite, because the initial positive charged fraction changed more rapidly, if the symmetric small ion concentrations were assumed in the iteration method. As a result, if $f^{+}_{\mathrm{ini,sim}}$ was overcharged, then a higher value of $f^{+}_{\mathrm{ini,iter}}$ was obtained with the iteration method when using symmetric small ion concentrations instead of asymmetric ones.

4.4.2 The initial charged fraction determined with the fitting method

The initial negative charged fractions from the fitting method, $f^{-}_{\mathrm{ini,fit}}$, as a function of simulated initial negative charged fractions, $f^{-}_{\mathrm{ini,sim}}$, are shown in Fig. 8. Regardless of whether the data points were from DR 1 or DR 2, there were results in all three categories. However, all the points in the undesired category 2 were from simulations in which $\mathrm{GR_{input}}$ was the smallest ($1\,\mathrm{nm\,h^{-1}}$) and/or growth rate scenario 2 was used.

Let us again have a more detailed look at the results belonging to the category 3. When the data points were from DR 2, the correspondence between $f^{-}_{\mathrm{ini,sim}}$ and $f^{-}_{\mathrm{ini,fit}}$ for the results in category 3 was poor (Fig. 8). The correspondence between $f^{-}_{\mathrm{ini,sim}}$ and $f^{-}_{\mathrm{ini,fit}}$ varied between the simulations with different growth rate scenarios, with $f^{-}_{\mathrm{ini,fit}}$ typically overestimating $f^{-}_{\mathrm{ini,sim}}$ when charged particles grew more rapidly than neutral ones (GR scenarios 2 and 3), and underestimating $f^{-}_{\mathrm{ini,sim}}$ otherwise.

If the data points were from DR 1, the correspondence between $f^{-}_{\mathrm{ini,sim}}$ and $f^{-}_{\mathrm{ini,fit}}$ for results in category 3 was much better than in the case of DR 2. Nevertheless, the values of $f^{-}_{\mathrm{ini,fit}}$ were considerably larger than the values of $f^{-}_{\mathrm{ini,sim}}$ for the simulations with growth rate scenario 3 and considerably smaller with growth rate scenario 4. Furthermore, in one third of the simulations with growth rate scenario 2, $f^{-}_{\mathrm{ini,fit}}$ overestimated $f^{-}_{\mathrm{ini,sim}}$ by at least a factor of 5. The results shown in Fig. 8 are only for $f^{-}_{\mathrm{ini,fit}}$, but the corresponding results for $f^{+}_{\mathrm{ini,fit}}$ were very similar.

If we now look at the results in category 3 shown in Fig. 8, there is a lot of variation in the values of $f^{-}_{\mathrm{ini,fit}}$ regardless of the values of $f^{-}_{\mathrm{ini,sim}}$, especially when using DR 2. This variation cannot be explained by whether or not the fitting method has taken into account the processes dominating the changes in the charged fraction (denoted by the colour of the points). We found out that varying the growth rate, the new particle

formation rate or the condensation sink all led to variation in $f^-_{\mathrm{ini,fit}}$. A high growth rate, low formation rate and low condensation sink were all required to significantly decrease the variation in $f^-_{\mathrm{ini,fit}}$ observed in Fig. 8. Furthermore, the correspondence between $f^-_{\mathrm{ini,fit}}$ and $f^-_{\mathrm{ini,sim}}$ was especially poor when $\mathrm{GR_{input}}$ was $1\,\mathrm{nm\,h^{-1}}$, since in those cases the information of the initial charged fraction was minimal in the diameter range of the data points.

4.5 Implications to analysis of measurement data

4.5.1 Suitability of the methods on various measurement conditions

In this study, we have analyzed simulated data covering a wide range of atmospheric conditions with the fitting and the iteration methods. When assessing whether these methods could be used to analyze data measured in specific conditions, there are two aspects that need to be taken into account.

Firstly, the condensational growth rate of the particles has to be sufficiently high, preferable at least $\sim 3\,\mathrm{nm\,h^{-1}}$. If the growth rate is small, the information of the initial charged fraction may have been lost before the particles reach the sizes covered by the measurements (Kerminen et al., 2007). Furthermore, with small growth rates, the measured charged fractions are close to their value in equilibrium. In such conditions, any unexpected deviation of the measured charged fraction from the equilibrium value could cause misinterpretation of the growth rate. As a result, the methods are very susceptible to error sources, like inaccuracies in measurements, if the actual growth rate is small. For this reason, the fitting and the iteration methods cannot be used to obtain the growth rate that is used to justify the usage of these methods.

Secondly, the processes affecting the charged fraction taken into account in the methods described in this work are ion-aerosol attachment (fitting and iteration method) and intramodal recombination (fitting method). If the concentration of nucleation mode particles and/or larger pre-existing particles is sufficiently large, then intramodal coagulation and/or coagulation scavenging have to be taken into account also. This is typically the case in polluted environments.

We have selected a few measurement sites described in detail by Manninen et al. (2010) and assessed whether or not the iteration and the fitting methods could be used on the data obtained at those sites (Table 4). The sites were chosen to represent different kinds of environments, but they do not represent tropospheric conditions exhaustively. The assessment is based on typical values observed at the sites and does not necessarily hold for every new particle formation event measured at the sites. The assessment was made by estimating whether the methods took into account the processes dominating the changes in the charged fraction, represented by the value of $F^{\pm}$ (see Appendix B for details). The methods were assumed to be suitable as such if the value of $F^{\pm}$ was > 0.8 and growth rate was $> 3\,\mathrm{nm\,h^{-1}}$.

The values observed in the measurements that were used for assessing the suitability of the methods for analyzing the data from different measurement sites are presented in Table 4. The values of concentrations and growth rates are medians over the new particle formation event days observed during the time period of the EUCAARI campaign (Manninen et al., 2010), except for Hyytiälä, for which the time period from 1 March to 30 June 2007 was used. From each event day, only data from 09:00 to 15:00 were used, since the events occurred mostly during that time. The values of condensation sink are according to Manninen et al. (2010).

The growth rates presented in Table 4 were determined by following the centre of the nucleation mode (Lehtinen and Kulmala, 2003; Hirsikko et al., 2005) over a diameter range from 3 to 7 nm. This was achieved by estimating the moment of the highest particle number concentration in each of the size sections in that diameter range and fitting a straight line to these data points with the growth rate obtained as the slope of the line. This method is only suitable for analyzing regional new particle formation events. For this reason, the coastal events measured at Mace Head were omitted here. The growth rates during the coastal events can be several hundreds of nm per hour (O'Dowd et al., 2002), but the growth conditions change rapidly during the transition from the place of the actual particle formation to the measurement site. Whether the iteration and the fitting methods are suitable for analyzing the coastal events or not is beyond the scope of this study.

The concentrations were obtained from measurements with the Neutral cluster and Air Ion Spectrometer (NAIS, Kulmala et al., 2007). The NAIS instrument can measure the total particle concentration using negative or positive corona discharging of the particle sample and thus two estimates on the total concentration are obtained. The value of total concentration presented in Table 4 for each site is the one based on negative polarity, while the corresponding values based on positive polarity were very similar. The values of the concentrations given in Table 4 represent the same days for which the growth rates were determined. The number of such days for each of the sites is also given in Table 4.

4.5.2 Case study on the conditions similar to those observed at the SMEAR II station

The values used as input in the simulations (Table 1) covered a wide range of atmospheric conditions. Let us now focus on only a few of the simulations with the conditions closest to those observed at SMEAR II station in Hyytiälä, southern Finland (Hari and Kulmala, 2005), where the fitting method has previously been used (e.g. Laakso et al., 2007a). The following values were chosen to represent the typical conditions at Hyytiälä: $\mathrm{GR_{input}} = 3\,\mathrm{nm\,h^{-1}}$, $J_{1.8} = 1\,\mathrm{cm^{-3}\,s^{-1}}$ and $\mathrm{CS} = 1 \times 10^{-3}\,\mathrm{s^{-1}}$, where $J_{1.8}$ is the formation rate of 1.8-nm particles. The growth rate has been observed to increase as a function of diameter at Hyytiälä (Hirsikko et al.,

Table 4. The values of growth rate (GR), condensation sink (CS), concentrations of small ions ($N_C^{\pm}$) and concentrations of total (neutral + charged) and charged nucleation mode particles (N^{tot} and $N^{\pm}$) from five measurement sites. The values were used to assess whether or not the iteration and the fitting method would be suitable for data analysis in these particular conditions: A = suitable as such, B = coagulation processes need to be added to the method, C = not suitable due to coagulation processes, D = not suitable due to too small growth rate. If the assessment was different for the negative and positive polarity, both of them are presented in the table (negative/positive polarity).

	Hyytiälä	Pallas	Melpitz	Mace Head	Jungfraujoch
# of events	24	6	29	6	9
GR (nm h^{-1})	3.0	5.6	5.7	2.7	7.2
CS (s^{-1})	1.4×10^{-3}	6.3×10^{-4}	8.4×10^{-3}	6.4×10^{-4}	5.9×10^{-4}
N_C^- (cm^{-3})	830	520	340	450	440
N_C^+ (cm^{-3})	710	620	290	480	940
N^{tot} (cm^{-3})	5300	2700	25 000	15 000	2700
N^- (cm^{-3})	160	140	570	340	120
N^+ (cm^{-3})	120	140	530	810	110
Fitting	A	A	C	D	A
Iteration	B/A	A	B	D	A

2005; Yli-Juuti et al., 2011) and the condensational growth of charged particles is likely to be at least moderately enhanced compared to that of the neutral ones. For this reason, we considered here only simulations with either GR scenario 3 (moderately enhanced growth of charged particles) or GR scenario 4 (growth rate increased as a function of diameter). All of the six combinations of fractions of IIN used as input in the model were considered and so, the total number of considered simulations was twelve.

The values of IIN used as input in the model, initial charged fractions observed in the simulations and the initial charged fractions determined with the iteration and fitting methods are given in Table 5. In majority of these simulations both the iteration and the fitting method took into account the processes dominating the changes in the charged fraction, i.e. the value of $F^{\pm}$ was close to unity (Table 5). The only notable exception was the iteration method in simulations with high fraction of IIN used as input in the model, for which values of $F^{\pm} < 0.65$ were observed. In other cases, according to the assessment procedure described in Sect. 4.5.1, the usability of the methods depended on the growth rate, which will be looked into in more detail below.

For the simulations in which the fraction of IIN was > 0.5 % and GR scenario 3 (scenario 4) was used, the initial charged fractions observed in the simulations were approximately 40 % (20 %) smaller than the corresponding fractions of IIN used as input in the model (Table 5). Here, the initial charged fractions determined with the methods will be compared with the values of IIN used as input in the model. This will be done to provide results that are relevant from the point of view of the atmospheric measurements (Laakso et al., 2007a, b; Gagné et al., 2008, 2010, 2012).

If data points from DR 1 (2.2–11.5 nm) were used when analyzing the simulated data, both of the methods were able to give reasonable estimates of the initial charged fractions. If the fraction of IIN was 0.5 % or less, the initial charged fractions estimated with the methods were typically below 1 %. Otherwise, regardless of whether the iteration or the fitting method was used, the ratio of the determined initial charged fraction to the value of fraction of IIN was approximately 0.7, i.e. the methods underestimated the fraction of IIN by approximately 30 %.

If the data points were from DR 2 (3.0–11.5 nm) and if GR scenario 3 was used in the simulations, the ratios of the determined initial charged fraction and the value of fraction of IIN were ~ 0.95 and ~ 1.2 for the fitting and iteration methods, respectively. In other words, the fitting method underestimated the fraction of IIN by only ~ 5 % and the iteration method overestimated it by ~ 20 %. However, if GR scenario 4 was used in the simulation, the methods were not able to trustfully determine the fraction of IIN. The reason for this was that the growth rate was too small for the particle population to bear considerable amount of information of the initial charged fraction at 3 nm. The average growth rates in simulations with $\text{GR}_{\text{input}} = 3\,\text{nm h}^{-1}$ and using GR scenario 4 for diameter ranges < 3 nm, 3–7 nm and 7–20 nm were 1.3, 2.2 and 2.9 nm h^{-1}, respectively (Fig. 1). The corresponding growth rates observed at Hyytiälä are 1.9, 3.8 and 4.3 nm h^{-1}, respectively (Yli-Juuti et al., 2011). In other words, the growth rates observed in the measurements are on average ~ 1.5 times higher than the corresponding growth rates in these simulations. With the average growth rates observed at Hyytiälä, the particle population still bears information of the initial charged fraction at the sizes of DR 2. However, according to the observed variation in the growth rates, there are also nucleation events observed at Hyytiälä in which the growth rate is not sufficiently high for this information to exist at the sizes of DR 2.

The ratio of the initial charged fraction determined with either the fitting or the iteration method to the fraction of IIN

Table 5. The values of initial charged fractions determined with the fitting and the iteration methods for simulations with the values used as input in the model representing typical conditions at Hyytiälä, Finland. In these simulations, the particle growth rate (GR_{input}), condensation sink and new particle formation rates were $3\,nm\,h^{-1}$, $1\times10^{-3}\,s^{-1}$ and $1\,cm^{-3}\,s^{-1}$, respectively. All six combinations of fractions of IIN were used as well as GR scenarios 3 (growth rate of charged particles was moderately enhanced) and 4 (growth rate increased as a function of diameter). DR 1 and DR 2 denote the diameter ranges 1 (2.2–11.5 nm) and 2 (3–11.5 nm), respectively.

Method	f_{ini}^{-} (%)	f_{ini}^{+} (%)	IIN^{-} (%)	IIN^{+} (%)	f_{sim}^{-} (%)	f_{sim}^{+} (%)	F^{-}	F^{+}	GR scen.
Fitting, DR1 (DR2)	0.00 (0.01)	0.00 (0.00)	0	0	0.02	0.01	0.96	0.97	3
Iteration, DR1 (DR2)	0.00 (0.30)	0.01 (0.33)	0	0	0.02	0.01	0.93	0.95	3
Fitting, DR1 (DR2)	0.34 (0.59)	0.44 (0.82)	0	0	0.07	0.05	0.90	0.93	4
Iteration, DR1 (DR2)	0.50 (1.3)	0.65 (1.7)	0	0	0.07	0.05	0.84	0.88	4
Fitting, DR1 (DR2)	3.0 (3.9)	3.0 (4.0)	5	5	2.3	2.3	0.93	0.95	3
Iteration, DR1 (DR2)	3.7 (6.6)	3.8 (6.4)	5	5	2.3	2.3	0.82	0.82	3
Fitting, DR1 (DR2)	2.4 (0.83)	2.4 (1.2)	5	5	3.9	4.1	0.88	0.91	4
Iteration, DR1 (DR2)	1.8 (1.8)	2.2 (2.3)	5	5	3.9	4.1	0.79	0.83	4
Fitting, DR1 (DR2)	47 (64)	47 (61)	50	50	48	48	0.98	0.99	3
Iteration, DR1 (DR2)	48 (61)	48 (59)	50	50	48	48	0.62	0.64	3
Fitting, DR1 (DR2)	43 (1.5)	46 (2.4)	50	50	43	45	0.95	0.96	4
Iteration, DR1 (DR2)	42 (3.2)	41 (4.4)	50	50	43	45	0.82	0.85	4
Fitting, DR1 (DR2)	1.8 (2.4)	0.00 (0.00)	3	0	1.3	0.01	0.90	0.98	3
Iteration, DR1 (DR2)	2.5 (4.3)	0.02 (0.31)	3	0	1.3	0.01	0.85	0.93	3
Fitting, DR1 (DR2)	1.1 (0.82)	0.42 (0.75)	3	0	2.4	0.05	0.85	0.94	4
Iteration, DR1 (DR2)	1.3 (1.8)	0.59 (1.6)	3	0	2.4	0.05	0.78	0.88	4
Fitting, DR1 (DR2)	6.1 (9.3)	0.25 (0.29)	10	0.5	4.6	0.24	0.95	0.97	3
Iteration, DR1 (DR2)	7.1 (13)	0.48 (0.76)	10	0.5	4.6	0.24	0.92	0.83	3
Fitting, DR1 (DR2)	6.1 (1.4)	0.53 (0.66)	10	0.5	7.8	0.45	0.90	0.94	4
Iteration, DR1 (DR2)	3.5 (2.7)	0.67 (1.4)	10	0.5	7.8	0.45	0.86	0.87	4
Fitting DR1 (DR2)	29 (40)	7.3 (8.5)	40	10	24	5.9	0.96	0.98	3
Iteration, DR1 (DR2)	30 (39)	6.9 (7.9)	40	10	24	5.9	0.86	0.57	3
Fitting, DR1 (DR2)	25 (3.3)	8.2 (0.70)	40	10	33	8.3	0.94	0.94	4
Iteration, DR1 (DR2)	22 (5.6)	4.3 (1.2)	40	10	33	8.3	0.90	0.79	4

used as input in the model varied between 0.36 and 1.43, excluding the situations with small fraction of IIN ($< 0.5\,\%$) or too small growth rate. Thus, as a conservative estimate, the iteration and the fitting methods were able to determine the fraction of IIN within a factor of 3 in the conditions that were chosen to represent those observed at Hyytiälä. This estimate holds only for cases with the growth rate similar to or above the average value observed in the measurements, and it does not include uncertainties related to measurements. It should be noted that other methods have also been used to determine the fraction of IIN (Manninen et al., 2010), but assessing the precision of those methods is beyond the scope of this paper.

5 Summary and conclusions

The fraction of particles formed carrying an electric charge varies between different atmospheric conditions. Regardless of the initial fraction, the fraction of charged particles approaches a value indicative of charge equilibrium as the particles grow to larger sizes. The measurements of aerosol charging state and charged fraction can be used to estimate the particle diameter growth rate and the initial fraction of charged particles, provided that the dynamic processes governing the change in the fraction of charged particles are known sufficiently well.

We conducted a set of aerosol dynamics simulations with varying conditions similar to those observed in the atmosphere. We then estimated the particle growth rate and the initial charged fractions from the simulated data using the iteration and the fitting method that have previously been used on measured data. The estimated values were compared with the corresponding simulated values and the methods were found to be able to give reasonable estimates with certain restrictions on the conditions.

We found that if charged particles grew much more rapidly than neutral ones (an enhancement factor of ~ 10 at a diameter of ~ 2 nm), the methods were not able to reasonably estimate either the growth rate or the initial charged fraction. If the growth rate of charged particles was moderately enhanced compared to that of neutral ones (an enhancement of ~ 2 at a diameter of ~ 2 nm), or the growth rate of all particles was diameter dependent, the correspondence between the simulated and the estimated growth rate was typically as good as, or only slightly worse than, in the case of all

particles growing by the same rate regardless of their size or charge.

When the particle growth rate was small ($< 3\,\mathrm{nm\,h^{-1}}$), the methods were found to be very sensitive to processes that were not taken into account in the methods. We would advice that neither the iteration nor the fitting method should be used for analysing the aerosol charging state when the charged particles grow much more rapidly than neutral ones and/or if the condensational growth rate is small ($< 3\,\mathrm{nm\,h^{-1}}$). Here it should be noted that the values of growth rate obtained with the iteration or fitting methods themselves cannot be used to justify the usage of the methods, since they do not provide trustworthy estimates of the growth rate when the actual growth rate is very small.

We found that even a relatively small difference, or asymmetry, in the small ion concentrations (600 and $800\,\mathrm{cm^{-3}}$, for negative and positive small ions, respectively) should be taken into account in the iteration method. If the small ion concentrations were assumed to be the same in the analysis, a considerable overestimation of the simulated growth rate was observed, especially if the simulated growth rate was small.

The data points of the charged fraction below 3 nm in diameter were found to improve significantly the correspondence between the estimated and the simulated charged fraction at 1.8 nm. However, the correspondence between the estimated and the simulated growth rate worsened when data points below 3 nm were used, especially if charged particles grew more rapidly than neutral ones.

The suitability of these methods for analysis of measurement data depends on the conditions at the measurement site and should be checked individually for different conditions. We have provided a simple way of estimating whether the methods take into account the processes dominating the changes in the charged fraction in particular conditions and assessed the suitability of the methods in a few example cases. With a high enough condensation sink and/or a high enough concentration of nucleation mode particles, the coagulation processes have to be included in the methods. Inclusion of coagulation processes to the iteration method has already been done by Iida et al. (2008) in the charge symmetric framework, but not in the asymmetric frame work used in this study. The inclusion of the coagulation processes to the iteration method in the asymmetric framework is beyond the scope of this study, but it could be done in the future.

Appendix A

Comparison of the initial charged fraction determined with the iteration method to the fraction of IIN used as input in the model

In Sect. 4.1 we demonstrated that the initial charged fraction in the simulations, $f^{\pm}_{\mathrm{ini,sim}}$, did not equal the fraction of particles formed via ion-induced nucleation, $\mathrm{IIN}^{\pm}$. The iteration and fitting methods, described in Sects. 2.2.1 and 2.2.2, are able to provide estimates on the initial charged fraction at the size the particles are assumed to be formed, but in order to estimate the fraction of $\mathrm{IIN}^{\pm}$, the differences in the removal rates of the neutral and charged particles need to be taken into account.

Since it is beyond the scope of this study to assess how the fraction of $\mathrm{IIN}^{\pm}$ should be estimated from the initial charged fraction, we evaluated the performance of the iteration and fitting methods by comparing the initial charged fractions determined using the methods to those obtained directly from the simulations. However, in previous studies the initial charged fraction has been assumed to be equal to the fraction of $\mathrm{IIN}^{\pm}$ (Laakso et al., 2007a; Gagné et al. 2008, 2010, 2012). In order to estimate the accuracy of those studies, we also compared the initial charged fractions determined with the iteration and fitting methods to the corresponding fractions of IIN used as input in the model. The results of that comparison are shown here only for the negative initial charged fraction determined with the iteration method. The corresponding results for the fitting method and for the positive initial charged fraction determined with either of the methods were very similar.

When comparing the initial charged fractions determined with the iteration and fitting methods to the corresponding values in the simulations, the results were divided into three categories defined in Sect. 4.4. According to that definition, category 3 included results of the simulations in which $f^{\pm}_{\mathrm{ini,sim}} > 1\,\%$. When comparing the initial charged fractions determined with the methods to the corresponding proportion of IIN used as input in the model, the definition of category 3 was adapted to include results of the simulations in which $\mathrm{IIN}^{\pm} > 1\,\%$.

The initial negative charged fractions determined with the iteration method with asymmetric small ion concentrations, $f^{-}_{\mathrm{ini,iter}}$, as a function of corresponding proportion of IIN^{-}, are shown in Fig. A1. The data points with the value of $\mathrm{IIN}^{-} = 0\,\%$ were omitted from the figure, but for the vast majority of those cases either the value of $f^{-}_{\mathrm{ini,iter}}$ was $< 1\,\%$ or the growth rate used as input in the model was $1\,\mathrm{nm\,h^{-1}}$. When comparing the results in category 3 shown in Figs. 7 and A1, the largest difference can be observed in the distribution of points for the simulations with the growth rate scenario 2. The general shapes of the curves corresponding to the simulations with GR scenario 2 were much more similar to the shapes of the other curves in Fig. A1 than in Fig. 7 (panels C and D). It should be noted that the number of data points in category 3 for simulations with GR scenario 2 is much higher in Fig. A1 than in Fig. 7, because, in those simulations, the proportion of IIN^{-} was typically much larger than $f^{-}_{\mathrm{ini,sim}}$ (Fig. 2).

Regardless of GR scenario used in the simulation, the iteration method underestimated the proportion of IIN^{-} (Fig. A1) slightly more often than it underestimated $f^{-}_{\mathrm{ini,sim}}$

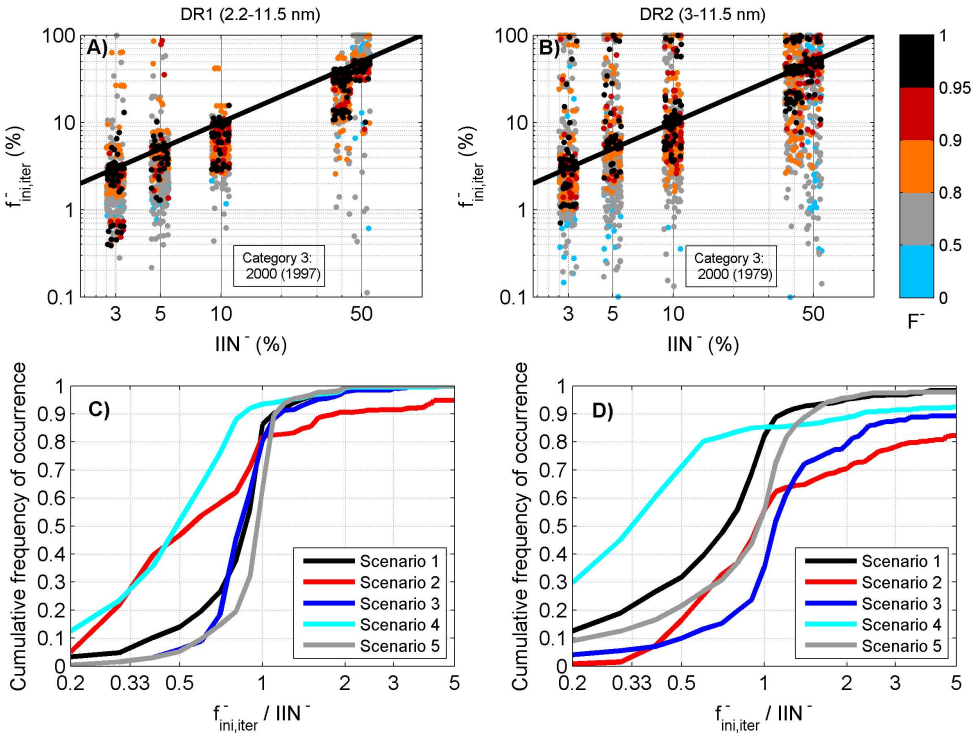

Fig. A1. The initial negative charged fractions determined with the iteration method using asymmetric small ion concentrations as a function of the proportion of IIN^- used as input in the model are depicted in the upper panels. The colour denotes the fraction of the change rate of the negative charged fraction that was taken into account in the method (see details in Appendix B). The solid black line denotes the one to one correspondence. The numbers denote the number of data points in category 3 with the numbers in parenthesis denoting the number of data points shown in the figure. The points not shown in the figure had the value of $f^-_{\mathrm{ini,iter}} < 0.1\,\%$. The cumulative frequency of occurrence of the ratio of the determined charged fraction and the fraction of IIN^- are depicted in the lower panels with different colours denoting different GR scenarios used in the simulations. All of the data points in category 3 were used to obtain the curves in **(C)** and **(D)**. The panels on the left (**A** and **C**) and right hand side (**B** and **D**) denote the results obtained using data from DR 1 (2.2–11.5 nm) and DR 2 (3–11.5 nm), respectively. A random variation of up to 10 % is added to the values on the x-axis of **(A)** and **(B)** to make data points more distinguishable.

(Fig. 7). This behaviour was expected since $f^{\pm}_{\mathrm{ini,sim}} < IIN^{\pm}$ (Fig. 2). The difference was not very big, however, except for the simulations in which the charged particles grew more rapidly than the neutral ones (GR scenarios 2 and 3).

When analysing data measured at SMEAR II station in Hyytiälä, different studies using different approaches have ended up to different conclusions on the importance of the particle formation mechanisms involving charges compared to purely neutral mechanisms. The fitting method described in Sect 2.2.1 was used in the studies by Laakso et al. (2007a) and Gagné et al. (2008, 2010, 2012) on the data measured with Ion-DMPS. In those studies, it was found that the new particle formation was rarely dominated by IIN with the median proportion of IIN being 6.4 % (Gagné et al., 2008). In the study by Manninen et al. (2009), the contribution of ion-mediated nucleation (IIN plus particles formed via recombination of oppositely-charged small ions) was estimated to be $\sim 10\,\%$ in Hyytiälä conditions using a data analysis method that is based on apparent formation rates of total and charged particles. However, Yu and Turco (2008, 2011) analyzed eight nucleation event days from spring 2005 with a kinetic aerosol dynamics model that uses ion-mediated nucleation, IMN, as the mechanism for particle formation and were able to match the charged fractions at 2 nm as estimated by Laakso et al. (2007a), at least within reasonable uncertainties. The conclusions on the importance of IMN of the studies listed above seem contradicting, and though it is not a major motivation of this study, a few aspects can be pointed out to explain the difference.

First of all, the particle population may not bear memory of the initial charged fraction in the sizes of the measurements as explained by Kerminen et al. (2007). Since the loss of information is not a feature of the data analysis methods, but a consequence of physical processes, none of the methods listed above can give any estimate on the proportion of IIN in those cases. The memory effect has been considered in the study by Laakso et al. (2007a) and in studies by Gagné et al. (2008, 2010, 2012). It is likely that the loss of information of the initial charged fraction has occurred also in some of the eight cases analysed by Yu and Turco (2008, 2011).

Secondly, the assumption that the growth rate is constant regardless of the size and charge of the particle, which is assumed in the methods used by Laakso et al. (2007a), Gagné et al. (2008, 2010, 2012) and Manninen et al. (2009, 2010), may have a considerable effect on the estimated proportions of IIN. In this study, the fitting and iteration methods tended to underestimate the proportion of IIN when the growth rate increased as a function of diameter (Fig. A1). However, if the charged particles grew more rapidly than the neutral ones, the underestimation was decreased (Fig. A1). In Hyytiälä, the growth rate has been observed typically to increase as a function of diameter and the charged particles probably grow at least slightly more rapidly than the neutral ones. As a net effect, the iteration and fitting methods tend to somewhat underestimate the proportion of IIN when used on the data from Hyytiälä, but the magnitude of the underestimation is very much dependent on the growth rate. The method used by Manninen et al. (2009, 2010) is not considered in this study, but the results obtained using that method are most probably also affected by the size and charge dependence of the growth rate.

Furthermore, the charged fraction is very size dependent at sizes below 3 nm in diameter (Kerminen et al., 2007; Yu and Turco, 2011). This phenomenon introduces a considerable uncertainty when estimating the proportion of IIN, since the formation size of the particles is ambiguous.

Appendix B

Processes affecting the change rate of the charged fraction

Let us assume that we have a narrow nucleation mode, in which particles are either neutral or singly-charged. We approximate the nucleation mode using a monodisperse distribution, in which case the balance equations can be written as:

$$\frac{\mathrm{d}N^0}{\mathrm{d}t} = \alpha^- N_\mathrm{C}^- N^+ + \alpha^+ N_\mathrm{C}^+ N^- - \beta^- N_\mathrm{C}^- N^0 - \beta^+ N_\mathrm{C}^+ N^0 - 0.5 k_{0,0} \left(N^0\right)^2 - k_{0,-} N^0 N^- - k_{0,+} N^0 N^+ + k_{-,+} N^- N^+ - \mathrm{CoagS}_0 N^0 \quad \text{(B1a)}$$

$$\frac{\mathrm{d}N^-}{\mathrm{d}t} = -\alpha^+ N_\mathrm{C}^+ N^- + \beta^- N_\mathrm{C}^- N^0 - 0.5 k_{-,-} \left(N^-\right)^2 - k_{-,+} N^- N^+ - \mathrm{CoagS}_- N^- \quad \text{(B1b)}$$

$$\frac{\mathrm{d}N^+}{\mathrm{d}t} = -\alpha^- N_\mathrm{C}^- N^+ + \beta^+ N_\mathrm{C}^+ N^0 - 0.5 k_{+,+} \left(N^+\right)^2 - k_{-,+} N^- N^+ - \mathrm{CoagS}_+ N^+. \quad \text{(B1c)}$$

Here N^0, N^- and N^+ are the concentrations of neutral, negatively-charged and positively-charged particles, respectively, N_C^- and N_C^+ are the concentrations of negatively- and positively-charged small ions, respectively, $k_{0,0}$, $k_{0,\pm}$, $k_{\pm,\pm}$ and $k_{-,+}$ are the coagulation coefficients between two neutral particles, between a neutral and a charged particle, between two similarly-charged particles and between two oppositely-charged particles, respectively. The CoagS_q terms denote the scavenging rate of the nucleation mode particles with the charge q (neutral, negatively- or positively-charged) due to coagulation with larger pre-existing particles.

The terms on the right hand side in Eqs. (B1a)–(B1c) can be divided into four categories: the terms from first to fourth in Eq. (B1a), as well as first and second terms in Eqs. (B1b) and (B1c), are related to ion-aerosol attachment. The terms from fifth to seventh in Eq. (B1a), as well as third terms in Eqs. (B1b) and (B1c), are related to self-coagulation, excluding recombination within the mode. The eighth term in Eq. (B1a) and the fourth terms in Eqs. (B1b) and (B1c) are related to recombination within the nucleation mode. The ninth term in Eq. (B1a) and the fifth terms in Eqs. (B1b) and (B1c) are related to coagulation scavenging.

The charged fraction, $f^\pm = N^\pm / N^\mathrm{tot}$, changes in time as the particle concentrations change:

$$\frac{\mathrm{d}f^-}{\mathrm{d}t} = \frac{\mathrm{d}}{\mathrm{d}t}\left(\frac{N^-}{N^\mathrm{tot}}\right) = \frac{1}{N^\mathrm{tot}}\frac{\mathrm{d}N^-}{\mathrm{d}t} - \frac{N^-}{(N^\mathrm{tot})^2}\left(\frac{\mathrm{d}N^-}{\mathrm{d}t} + \frac{\mathrm{d}N^+}{\mathrm{d}t} + \frac{\mathrm{d}N^0}{\mathrm{d}t}\right) \quad \text{(B2a)}$$

$$\frac{\mathrm{d}f^+}{\mathrm{d}t} = \frac{\mathrm{d}}{\mathrm{d}t}\left(\frac{N^+}{N^\mathrm{tot}}\right) = \frac{1}{N^\mathrm{tot}}\frac{\mathrm{d}N^+}{\mathrm{d}t} - \frac{N^+}{(N^\mathrm{tot})^2}\left(\frac{\mathrm{d}N^-}{\mathrm{d}t} + \frac{\mathrm{d}N^+}{\mathrm{d}t} + \frac{\mathrm{d}N^0}{\mathrm{d}t}\right), \quad \text{(B2b)}$$

where N^tot is the total concentration of nucleation mode particles. By combining Eqs. (B1) and (B2) we get expressions for the change rates of charged fractions. Furthermore, we can write the change rate of the charged fraction separately for the ion-aerosol attachment, recombination within the mode, self-coagulation (excluding recombination within the mode) and coagulation scavenging, in which case we get

$$\left(\frac{\mathrm{d}f^-}{\mathrm{d}t}\right)_\mathrm{IA} = \beta^- N_\mathrm{C}^- \left(1 - f^- - f^+\right) - \alpha^+ N_\mathrm{C}^+ f^- \quad \text{(B3a)}$$

$$\left(\frac{\mathrm{d}f^+}{\mathrm{d}t}\right)_\mathrm{IA} = \beta^+ N_\mathrm{C}^+ \left(1 - f^- - f^+\right) - \alpha^- N_\mathrm{C}^- f^+ \quad \text{(B3b)}$$

$$\left(\frac{\mathrm{d}f^-}{\mathrm{d}t}\right)_\mathrm{REC} = -k_{-,+} f^- N^+ \left(1 - f^-\right) \quad \text{(B4a)}$$

$$\left(\frac{\mathrm{d}f^+}{\mathrm{d}t}\right)_\mathrm{REC} = -k_{-,+} f^+ N^- \left(1 - f^+\right) \quad \text{(B4b)}$$

$$\left(\frac{\mathrm{d}f^-}{\mathrm{d}t}\right)_\mathrm{SC} = 0.5 k_{0,0} N^\mathrm{tot} f^- \left(1 - f^- - f^+\right)^2 + f^- \left(k_{0,-} f^- + k_{0,+} f^+\right) N^\mathrm{tot} \left(1 - f^- - f^+\right) \quad \text{(B5a)}$$

$$\left(\frac{\mathrm{d}f^+}{\mathrm{d}t}\right)_{\mathrm{SC}} = 0.5k_{0,0}N^{\mathrm{tot}}f^+\left(1-f^--f^+\right)^2 + f^+\left(k_{0,-}f^- + k_{0,+}f^+\right)N^{\mathrm{tot}}\left(1-f^--f^+\right) \quad \text{(B5b)}$$

$$\left(\frac{\mathrm{d}f^-}{\mathrm{d}t}\right)_{\mathrm{CS}} = -\mathrm{CoagS}_-f^-\left(1-f^-\right) + \mathrm{CoagS}_+f^+f^- + \mathrm{CoagS}_0f^-\left(1-f^--f^+\right) \quad \text{(B6a)}$$

$$\left(\frac{\mathrm{d}f^+}{\mathrm{d}t}\right)_{\mathrm{CS}} = -\mathrm{CoagS}_+f^+\left(1-f^+\right) + \mathrm{CoagS}_-f^+f^- + \mathrm{CoagS}_0f^+\left(1-f^--f^+\right) \quad \text{(B6b)}$$

Here IA, REC, SC and CS refer to ion-aerosol attachment, recombination within the nucleation mode, self-coagulation within the nucleation mode (excluding recombination) and coagulation scavenging, respectively.

In the form described by Gagné et al. (2012), the fitting method takes into account the ion-aerosol attachment and recombination within the mode, whereas the iteration method only takes into account the ion-aerosol attachment. Thus, the fraction of total change rate of the charged fraction taken into account in these two methods, $F^{\pm}_{\mathrm{fit}}(d_{\mathrm{p}})$ and $F^{\pm}_{\mathrm{iter}}(d_{\mathrm{p}})$ for fitting and iteration method, respectively, can be estimated as:

$$F^{\pm}_{\mathrm{fit}}\left(d_{\mathrm{p}}\right) = \frac{\left|\left(\frac{\mathrm{d}f^{\pm}}{\mathrm{d}t}\right)_{\mathrm{IA}}\left(d_{\mathrm{p}}\right)\right| + \left|\left(\frac{\mathrm{d}f^{\pm}}{\mathrm{d}t}\right)_{\mathrm{REC}}\left(d_{\mathrm{p}}\right)\right|}{\left|\left(\frac{\mathrm{d}f^{\pm}}{\mathrm{d}t}\right)_{\mathrm{IA}}\left(d_{\mathrm{p}}\right)\right| + \left|\left(\frac{\mathrm{d}f^{\pm}}{\mathrm{d}t}\right)_{\mathrm{REC}}\left(d_{\mathrm{p}}\right)\right| + \left|\left(\frac{\mathrm{d}f^{\pm}}{\mathrm{d}t}\right)_{\mathrm{CS}}\left(d_{\mathrm{p}}\right)\right| + \left|\left(\frac{\mathrm{d}f^{\pm}}{\mathrm{d}t}\right)_{\mathrm{SC}}\left(d_{\mathrm{p}}\right)\right|} \quad \text{(B7)}$$

and

$$F^{\pm}_{\mathrm{iter}}\left(d_{\mathrm{p}}\right) = \frac{\left|\left(\frac{\mathrm{d}f^{\pm}}{\mathrm{d}t}\right)_{\mathrm{IA}}\left(d_{\mathrm{p}}\right)\right|}{\left|\left(\frac{\mathrm{d}f^{\pm}}{\mathrm{d}t}\right)_{\mathrm{IA}}\left(d_{\mathrm{p}}\right)\right| + \left|\left(\frac{\mathrm{d}f^{\pm}}{\mathrm{d}t}\right)_{\mathrm{REC}}\left(d_{\mathrm{p}}\right)\right| + \left|\left(\frac{\mathrm{d}f^{\pm}}{\mathrm{d}t}\right)_{\mathrm{CS}}\left(d_{\mathrm{p}}\right)\right| + \left|\left(\frac{\mathrm{d}f^{\pm}}{\mathrm{d}t}\right)_{\mathrm{SC}}\left(d_{\mathrm{p}}\right)\right|}. \quad \text{(B8)}$$

It should be noted that depending on the conditions, the terms related to ion-aerosol attachment and coagulation scavenging can, at least in theory, be either negative or positive, whereas the terms related to intramodal recombination and self-coagulation are always negative and positive, respectively. However, by taking the absolute value of each of the terms, we limit the values of $F^{\pm}_{\mathrm{fit}}(d_{\mathrm{p}})$ and $F^{\pm}_{\mathrm{iter}}(d_{\mathrm{p}})$ to a range from 0 to 1, where values closer to unity mean that the method does take into account the processes dominating the changes in the charged fraction.

The values of $F^{\pm}_{\mathrm{fit}}(d_{\mathrm{p}})$ and $F^{\pm}_{\mathrm{iter}}(d_{\mathrm{p}})$ depend on the particle diameter and Eqs. (B1a)–(B8) hold only for monodisperse distributions. However, in the simulations conducted in this study, the simulated particle size range was from 1.8 to 20 nm and the concentrations of particles in different size sections varied in time. In order to simplify the analysis, we calculated only one value of $F^{\pm}_{\mathrm{fit}}$ and $F^{\pm}_{\mathrm{iter}}$ for each simulation. These values were calculated according to

$$F^{\pm}_{\mathrm{fit}} = \frac{\sum_{i=1}^{4}\left(\left|\left(\frac{\mathrm{d}f^{\pm}}{\mathrm{d}t}\right)_{\mathrm{IA}}\left(d_{\mathrm{p},i}\right)\right| + \left|\left(\frac{\mathrm{d}f^{\pm}}{\mathrm{d}t}\right)_{\mathrm{REC}}\left(d_{\mathrm{p},i}\right)\right|\right) \times \left(\frac{\mathrm{d}f^{\pm}}{\mathrm{d}t}\right)_{\mathrm{TOT}}\left(d_{\mathrm{p},i}\right)}{\sum_{i=1}^{4}\left(\frac{\mathrm{d}f^{\pm}}{\mathrm{d}t}\right)_{\mathrm{TOT}}\left(d_{\mathrm{p},i}\right)} \quad \text{(B9)}$$

and

$$F^{\pm}_{\mathrm{iter}} = \frac{\sum_{i=1}^{4}\left|\left(\frac{\mathrm{d}f^{\pm}}{\mathrm{d}t}\right)_{\mathrm{IA}}\left(d_{\mathrm{p},i}\right)\right| \times \left(\frac{\mathrm{d}f^{\pm}}{\mathrm{d}t}\right)_{\mathrm{TOT}}\left(d_{\mathrm{p},i}\right)}{\sum_{i=1}^{4}\left(\frac{\mathrm{d}f^{\pm}}{\mathrm{d}t}\right)_{\mathrm{TOT}}\left(d_{\mathrm{p},i}\right)} \quad \text{(B10)}$$

where $(\mathrm{d}f^{\pm}/\mathrm{d}t)_{\mathrm{TOT}}$ is the total change rate of the charged fraction and $d_{\mathrm{p},1}$, $d_{\mathrm{p},2}$, $d_{\mathrm{p},3}$ and $d_{\mathrm{p},4}$ are 2.2, 2.5, 3.0 and 3.9 nm, respectively. The values of terms on the right hand side of Eqs. (B9) and (B10) were calculated assuming that all the nucleation mode particles had the diameter $d_{\mathrm{p},i}$ during the moment of time in which the centre of the mode was at that size.

The fitting method was used only on the data of one polarity at the time and the value of $F^{\pm}_{\mathrm{fit}}$ of corresponding polarity was used in the analysis. For the iteration method, which was used simultaneously on both polarities, the value of F^{-}_{iter} was used.

When assessing the suitability of the fitting and the iteration methods for analyzing the data collected at different measurement sites (see Sect. 4.5.1), the values of $f^{\pm}(d_{\mathrm{p},i})$ were estimated based on the nucleation mode concentrations:

$$f^{\pm}\left(d_{\mathrm{p},i}\right) = \frac{N^{\pm}}{N^{\mathrm{tot}}} \quad \text{(B11)}$$

where $N^{\pm}$ and N^{tot} are the charged and total concentration, respectively, of 3–20 nm particles. Also, the values of CoagS_q were estimated from the values of CS by assuming the same relation between CS and CoagS_q that was observed in the simulations conducted in this study.

Acknowledgements. This work has been supported by European Commission 6th Framework program project EUCAARI, contract no. 036833-2 (EUCAARI), and by Academy of Finland project ComQuaCC: Computational research chain from quantum chemistry to climate change, project no. 135199. The support by the Academy of Finland Centre of Excellence program (project no. 211483, 211484 and 1118615) is also gratefully acknowledged.

Edited by: I. Riipinen

References

Birmili, W., Berresheim, H., Plass-Dülmer, C., Elste, T., Gilge, S., Wiedensohler, A., and Uhrner, U.: The Hohenpeissenberg aerosol formation experiment (HAFEX): a long-term study including size-resolved aerosol, H_2SO_4, OH, and monoterpenes measurements, Atmos. Chem. Phys., 3, 361–376, doi:10.5194/acp-3-361-2003, 2003.

Dal Maso, M., Kulmala, M., Riipinen, I., Wagner, R., Hussein, T., Aalto, P. P., and Lehtinen, K. E. J.: Formation and growth of fresh atmospheric aerosols: eight years of aerosol size distribution data from SMEAR II, Hyytiälä, Finland. Boreal Env. Res., 10, 323–336, 2005.

Dal Maso, M., Sogacheva, L., Aalto, P. P., Riipinen, I., Komppula, M., Tunved, P., Korhonen, L., Suur-Uski, V., Hirsikko, A., Kurtén, T., Kerminen, V.-M., Lihavainen, H., Viisanen, Y., Hansson, H. C., and Kulmala, M.: Aerosol size distribution measurements at four Nordic field stations: identification, analysis and trajectory analysis of new particle formation bursts, Tellus, 59B, 350–361, 2007.

Ehn, M., Junninen, H., Schobesberger, S., Manninen, H. E., Franchin, A., Sipilä, M., Petäjä, T., Kerminen, V.-M., Tammet, H., Mirme, A., Mirme, S., Hõrrak, U., Kulmala, M., and Worsnop, D. R.: An Instrumental Comparison of Mobility and Mass Measurements of Atmospheric Small Ions, Aerosol Sci. Technol, 45, 522–532, 2011.

Forster, P., Ramaswamy, V., Artaxo, P., Berntsen, T., Betts, R., Fahey, D. W., Haywood, J., Lean, J., Lowe, D. C., Myhre, G., Nganga, J., Prinn, R., Raga, G., Schulz, M., and Van Dorland, R.: Changes in Atmospheric Constituents and in Radiative Forcing, in: Climate Change 2007: The Physical Science Basis. Contribution of Working Group I to the Fourth Assessment Report of the Intergovernmental Panel on Climate Change, edited by: Solomon, S., Qin, D., Manning, M., Chen, Z., Marquis, M., Averyt, K. B., Tignor, M., and Miller, H. L., Cambridge University Press, Cambridge, United Kingdom and New York, NY, USA, 2007.

Gagné, S., Laakso, L., Petäjä, T., Kerminen, V.-M., and Kulmala, M.: Analysis of one year of Ion-DMPS data from the SMEAR II station, Finland, Tellus, 60B, 318–329, 2008.

Gagné, S., Nieminen, T., Kurtén, T., Manninen, H. E., Petäjä, T., Laakso, L., Kerminen, V.-M., Boy, M., and Kulmala, M.: Factors influencing the contribution of ion-induced nucleation in a boreal forest, Finland, Atmos. Chem. Phys., 10, 3743–3757, doi:10.5194/acp-10-3743-2010, 2010.

Gagné, S., Leppä, J., Petäjä, T., McGrath, M. J., Vana, M., Kerminen, V.-M., Laakso, L., and Kulmala, M.: Aerosol charging state at an urban site: new analytical approach and implications for ion-induced nucleation, Atmos. Chem. Phys., 12, 4647–4666, doi:10.5194/acp-12-4647-2012, 2012.

Gong, Y., Hu, M., Cheng, Y., Su, H., Yue, D., Liu, F., Wiedensohler, A., Wang, Z., Kalesse, H., Liu, S., Wu, Z., Xiao, K., Mi, P., and Zhang, Y.: Competition of coagulation sink and source rate: New particle formation in the Pearl River Delta of China, Atmos. Environ., 44, 3278–3285, 2010.

Hari, P. and Kulmala, M.: Station for Measuring Ecosystem-Atmosphere Relations (SMEAR II), Boreal Env. Res., 10, 315–322, 2005.

Held, A., Nowak, A., Birmili, W., Wiedensohler, A., Forkel, R., and Klemm, O.: Observations of particle formation and growth in a mountainous forest region in central Europe, J. Geophys. Res., 109, D23204, doi:10.1029/2004JD005346, 2004.

Hirsikko, A., Laakso, L., Hõrrak, U., Aalto, P. P., Kerminen, V.-M., and Kulmala, M.: Annual and size dependent variation of growth rates and ion concentrations in boreal forest, Boreal Env. Res., 10, 357–369, 2005.

Hirsikko, A., Nieminen, T., Gagné, S., Lehtipalo, K., Manninen, H. E., Ehn, M., Hõrrak, U., Kerminen, V.-M., Laakso, L., McMurry, P. H., Mirme, A., Mirme, S., Petäjä, T., Tammet, H., Vakkari, V., Vana, M., and Kulmala, M.: Atmospheric ions and nucleation: a review of observations, Atmos. Chem. Phys., 11, 767–798, doi:10.5194/acp-11-767-2011, 2011.

Iida, K., Stolzenburg, M. R., McMurry, P. H., and Smith, J. N.: Estimating nanoparticle growth rates from size-dependent charged fractions: Analysis of new particle formation events in Mexico City, J. Geophys. Res., 113, D05207, doi:10.1029/2007JD009260, 2008.

Kerminen, V.-M., Pirjola, L., and Kulmala, M.: How significantly does coagulational scavenging limit atmospheric particle production?, J. Geophys. Res., 106, 24119–24126, 2001.

Kerminen, V.-M., Anttila, T., Petäjä, T., Laakso, L., Gagné, S., Lehtinen, K. E. J., and Kulmala, M.: Charging state of the atmospheric nucleation mode: Implications for separating neutral and ion-induced nucleation, J. Geophys. Res., 112, D21205, doi:10.1029/2007JD008649, 2007.

Kerminen, V.-M., Petäjä, T., Manninen, H. E., Paasonen, P., Nieminen, T., Sipilä, M., Junninen, H., Ehn, M., Gagné, S., Laakso, L., Riipinen, I., Vehkamäki, H., Kurten, T., Ortega, I. K., Dal Maso, M., Brus, D., Hyvärinen, A., Lihavainen, H., Leppä, J., Lehtinen, K. E. J., Mirme, A., Mirme, S., Hõrrak, U., Berndt, T., Stratmann, F., Birmili, W., Wiedensohler, A., Metzger, A., Dommen, J., Baltensperger, U., Kiendler-Scharr, A., Mentel, T. F., Wildt, J., Winkler, P. M., Wagner, P. E., Petzold, A., Minikin, A., Plass-Dülmer, C., Pöschl, U., Laaksonen, A., and Kulmala, M.: Atmospheric nucleation: highlights of the EUCAARI project and future directions, Atmos. Chem. Phys., 10, 10829–10848, doi:10.5194/acp-10-10829-2010, 2010.

Kuang, C., McMurry, P. H., and McCormick, A. V.: Determination of cloud condensation nuclei production from measured new particle formation events, Geophys. Res. Lett., 36, L09822, doi:10.1029/2009GL037584, 2009.

Kuang, C., Chen, M., Zhao, J., Smith, J., McMurry, P. H., and Wang, J.: Size and time-resolved growth rate measurements of 1 to 5 nm freshly formed atmospheric nuclei, Atmos. Chem. Phys., 12, 3573–3589, doi:10.5194/acp-12-3573-2012, 2012.

Kulmala, M. and Kerminen, V.-M.: On the formation and growth of atmospheric nanoparticles, Atmos. Res., 90, 132–150, 2008.

Kulmala, M., Riipinen, I., Sipilä, M., Manninen, H. E., Petäjä, T., Junninen, H., Dal Maso, M., Mordas, G., Mirme, A., Vana, M., Hirsikko, A., Laakso, L., Harrison, R. M., Hanson, I., Leung, C., Lehtinen, K. E. J., and Kerminen, V.-M.: Towards direct measurements of atmospheric nucleation, Science, 318, 89–92, 2007.

Kulmala, M., Asmi, A., Lappalainen, H. K., Baltensperger, U., Brenguier, J.-L., Facchini, M. C., Hansson, H.-C., Hov, Ø., O'Dowd, C. D., Pöschl, U., Wiedensohler, A., Boers, R., Boucher, O., de Leeuw, G., Denier van der Gon, H. A. C., Feichter, J., Krejci, R., Laj, P., Lihavainen, H., Lohmann, U., McFiggans, G., Mentel, T., Pilinis, C., Riipinen, I., Schulz, M., Stohl, A., Swietlicki, E., Vignati, E., Alves, C., Amann, M.,

Ammann, M., Arabas, S., Artaxo, P., Baars, H., Beddows, D. C. S., Bergström, R., Beukes, J. P., Bilde, M., Burkhart, J. F., Canonaco, F., Clegg, S. L., Coe, H., Crumeyrolle, S., D'Anna, B., Decesari, S., Gilardoni, S., Fischer, M., Fjaeraa, A. M., Fountoukis, C., George, C., Gomes, L., Halloran, P., Hamburger, T., Harrison, R. M., Herrmann, H., Hoffmann, T., Hoose, C., Hu, M., Hyvärinen, A., Hõrrak, U., Iinuma, Y., Iversen, T., Josipovic, M., Kanakidou, M., Kiendler-Scharr, A., Kirkevåg, A., Kiss, G., Klimont, Z., Kolmonen, P., Komppula, M., Kristjánsson, J.-E., Laakso, L., Laaksonen, A., Labonnote, L., Lanz, V. A., Lehtinen, K. E. J., Rizzo, L. V., Makkonen, R., Manninen, H. E., McMeeking, G., Merikanto, J., Minikin, A., Mirme, S., Morgan, W. T., Nemitz, E., O'Donnell, D., Panwar, T. S., Pawlowska, H., Petzold, A., Pienaar, J. J., Pio, C., Plass-Duelmer, C., Prévôt, A. S. H., Pryor, S., Reddington, C. L., Roberts, G., Rosenfeld, D., Schwarz, J., Seland, Ø., Sellegri, K., Shen, X. J., Shiraiwa, M., Siebert, H., Sierau, B., Simpson, D., Sun, J. Y., Topping, D., Tunved, P., Vaattovaara, P., Vakkari, V., Veefkind, J. P., Visschedijk, A., Vuollekoski, H., Vuolo, R., Wehner, B., Wildt, J., Woodward, S., Worsnop, D. R., van Zadelhoff, G.-J., Zardini, A. A., Zhang, K., van Zyl, P. G., Kerminen, V.-M., S Carslaw, K., and Pandis, S. N.: General overview: European Integrated project on Aerosol Cloud Climate and Air Quality interactions (EUCAARI) – integrating aerosol research from nano to global scales, Atmos. Chem. Phys., 11, 13061–13143, doi:10.5194/acp-11-13061-2011, 2011.

Laakso, L., Gagné, S., Petäjä, T., Hirsikko, A., Aalto, P. P., Kulmala, M., and Kerminen, V.-M.: Detecting charging state of ultrafine particles: instrumental development and ambient measurements, Atmos. Chem. Phys., 7, 1333–1345, doi:10.5194/acp-7-1333-2007, 2007a.

Laakso, L., Grönholm, T., Kulmala, L., Haapanala, S., Hirsikko, A., Lovejoy, E. R., Kazil, J., Kurtén, T., Boy, M., Nilsson, E. D., Sogachev, A., Riipinen, I., Stratmann, F., and Kulmala, M.: Hot-air balloon as a platform for boundary layer profile measurements during particle formation, Boreal Environ. Res., 12, 279–294, 2007b.

Lehtinen, K. E. J. and Kulmala, M.: A model for particle formation and growth in the atmosphere with molecular resolution in size, Atmos. Chem. Phys., 3, 251–257, doi:10.5194/acp-3-251-2003, 2003.

Lehtinen, K. E. J., Dal Maso, M., Kulmala, M., and Kerminen, V.-M.: Estimating nucleation rates from apparent particle formation rates and vice versa: Revised formulation of the Kerminen-Kulmala equation, J. Aerosol Sci., 38, 988–994, 2007.

Leppä, J., Kerminen, V.-M., Laakso, L., Korhonen, H., Lehtinen, K. E. J., Gagné, S., Manninen, H. E., Nieminen, T., and Kulmala, M.: Ion-UHMA: a model for simulating the dynamics of neutral and charged aerosol particles, Boreal Env. Res., 14, 559–575, 2009.

Leppä, J., Anttila, T., Kerminen, V.-M., Kulmala, M., and Lehtinen, K. E. J.: Atmospheric new particle formation: real and apparent growth of neutral and charged particles, Atmos. Chem. Phys., 11, 4939–4955, doi:10.5194/acp-11-4939-2011, 2011.

Lushnikov, A. A. and Kulmala, M.: Charging of aerosol particles in the near free-molecule regime, Eur. Phys. J., D 29, 345–355, 2004.

Manninen, H. E., Nieminen, T., Riipinen, I., Yli-Juuti, T., Gagné, S., Asmi, E., Aalto, P. P., Petäjä, T., Kerminen, V.-M., and Kulmala, M.: Charged and total particle formation and growth rates during EUCAARI 2007 campaign in Hyytiälä, Atmos. Chem. Phys., 9, 4077–4089, doi:10.5194/acp-9-4077-2009, 2009.

Manninen, H. E., Nieminen, T., Asmi, E., Gagné, S., Häkkinen, S., Lehtipalo, K., Aalto, P., Vana, M., Mirme, A., Mirme, S., Hõrrak, U., Plass-Dülmer, C., Stange, G., Kiss, G., Hoffer, A., Töro, N., Moerman, M., Henzing, B., de Leeuw, G., Brinkenberg, M., Kouvarakis, G. N., Bougiatioti, A., Mihalopoulos, N., O'Dowd, C., Ceburnis, D., Arneth, A., Svenningsson, B., Swietlicki, E., Tarozzi, L., Decesari, S., Facchini, M. C., Birmili, W., Sonntag, A., Wiedensohler, A., Boulon, J., Sellegri, K., Laj, P., Gysel, M., Bukowiecki, N., Weingartner, E., Wehrle, G., Laaksonen, A., Hamed, A., Joutsensaari, J., Petäjä, T., Kerminen, V.-M., and Kulmala, M.: EUCAARI ion spectrometer measurements at 12 European sites – analysis of new particle formation events, Atmos. Chem. Phys., 10, 7907–7927, doi:10.5194/acp-10-7907-2010, 2010.

Mönkkönen, P., Koponen, I. K., Lehtinen, K. E. J., Hämeri, K., Uma, R., and Kulmala, M.: Measurements in a highly polluted Asian mega city: observations of aerosol number size distribution, modal parameters and nucleation events, Atmos. Chem. Phys., 5, 57–66, doi:10.5194/acp-5-57-2005, 2005.

Nadykto, A. B. and Yu, F.: Uptake of neutral polar vapor molecules by charged clusters/particles: Enhancement due to dipole-charge interaction, J. Geophys. Res., 108, 4717, doi:10.1029/2003JD003664, 2003.

Nieminen, T., Lehtinen, K. E. J., and Kulmala, M.: Sub-10 nm particle growth by vapor condensation – effects of vapor molecule size and particle thermal speed, Atmos. Chem. Phys., 10, 9773–9779, doi:10.5194/acp-10-9773-2010, 2010.

Nolan, P. J.: The Recombination Law for Weak Ionization, Nature, 148, 26, 1941.

O'Dowd, C. D., Hämeri, K., Mäkelä, J. M., Väkeva, M., Aalto, P. P., de Leeuw, G., Kunz, G. J., Becker, E., Hansson, H.-C., Allen, A. G., Harrion, R. M., Berresheim, H., Kleefeld, C., Geever, M., Jennings, S. G., and Kulmala M.: Coastal new particle formation: Environmental conditions and aerosol physico-chemical characteristics during nucleation bursts, J. Geophys. Res., 107, 8107, doi:10.1029/2000JD000206, 2002.

Pierce, J. R. and Adams, P. J.: Efficiency of cloud condensation nuclei formation from ultrafine particles, Atmos. Chem. Phys., 7, 1367–1379, doi:10.5194/acp-7-1367-2007, 2007.

Seinfeld, J. H. and Pandis, S. N.: Atmospheric Chemistry and Physics: From air pollution to climate change, John Wiley & Sons, 2006.

Spracklen, D. V., Carslaw, K. S., Kulmala, M., Kerminen, V.-M., Mann, G. W., and Sihto, S.-L.: The contribution of boundary layer nucleation events to total particle concentrations on regional and global scales, Atmos. Chem. Phys., 6, 5631–5648, doi:10.5194/acp-6-5631-2006, 2006.

Winkler, P. M., Steiner, G., Virtala, A., Vehkamäki, H., Noppel, M., Lehtinen, K. E. J., Reischl, G. P., Wagner, P. E., and Kulmala, M.: Heterogeneous Nucleation Experiments Bridging the Scale from Molecular Ion Clusters to Nanoparticles, Science, 319, 1374, doi:10.1126/science.1149034, 2008.

Yli-Juuti, T., Nieminen, T., Hirsikko, A., Aalto, P. P., Asmi, E., Hõrrak, U., Manninen, H. E., Patokoski, J., Dal Maso, M., Petäjä, T., Rinne, J., Kulmala, M., and Riipinen, I.: Growth rates of nucleation mode particles in Hyytiälä during 2003–

2009: variation with particle size, season, data analysis method and ambient conditions, Atmos. Chem. Phys., 11, 12865–12886, doi:10.5194/acp-11-12865-2011, 2011.

Yu, F. and Turco, R.: Case studies of particle formation events observed in boreal forests: implications for nucleation mechanisms, Atmos. Chem. Phys., 8, 6085–6102, doi:10.5194/acp-8-6085-2008, 2008.

Yu, F. and Turco, R. P.: The size-dependent charge fraction of sub-3-nm particles as a key diagnostic of competitive nucleation mechanisms under atmospheric conditions, Atmos. Chem. Phys., 11, 9451–9463, doi:10.5194/acp-11-9451-2011, 2011.

Yu, F., Luo, G., Bates, T. S., Anderson, B., Clarke, A., Kapustin, V., Yantosca, R. M., Wang, Y., and Wu, S.: Spatial distributions of particle number concentrations in the global troposphere: Simulations, observations, and implications for nucleation mechanisms, J. Geophys. Res., 115, D17205, doi:10.1029/2009JD013473, 2010.